Ph.D. Dissertation of Engineering

Development of a 3D Urban Surface Model for Evaluating Cooling Effect of Green Infrastructure

그린인프라의 냉각 효과 평가를 위한

3차원 도시 표면 모델 개발

August 2023

Graduate School of Seoul National University

Interdisciplinary Program in Landscape Architecture

Integrated Major in Smart City Global Convergence Program

Seok Hwan Yun

Development of a 3D urban surface model for evaluating cooling effect of green infrastructure

Advisor: Dong Kun Lee

A dissertation submitted in partial fulfillment of the requirements for the Degree of Doctor of Philosophy in Interdisciplinary Program in Landscape Architecture and Integrated Major in Smart City Global Convergence Program in Seoul National University

August 2023

Seok Hwan Yun

Approved by Thesis Committee

Chair __________________________(Seal)

Vice Chair__________________________(Seal)

Examiner __________________________(Seal)

Examiner __________________________(Seal)

Examiner __________________________(Seal)

Abstract

Development of a 3D urban surface model for evaluating cooling effect of green infrastructure

Seok Hwan Yun
Interdisciplinary Program in Landscape Architecture and
Integrated Major in Smart City Global Convergence Program in
Seoul National University
Graduate School of Seoul National University
Supervised by Professor Dong Kun Lee

The ongoing urbanization around the world is causing a lot of problems. One prominent issue is the urban heat island effect, exacerbated by climate change, which presents a significant challenge in understanding urban heat problems. The urban heat environment varies based on various factors such as climate, urban form, size, density, and surface materials. Consequently, different cities require distinct heat mitigation strategies, demanding a quantitative assessment of complex urban environments and cooling strategies.

Based on measurement research for quantitative evaluation, recent research is being conducted in the direction of complementing each other through simulation the shortcomings of limited time and space in connection with modeling However, in order to accurately simulate the cooling effect

and thermal environment, a three-dimensional urban canopy model that can comprehensively reflect various urban spaces is needed.

In this paper, 3D-USM was developed to diagnose the thermal environment of the city and evaluate the cooling effect of the green infrastructure to simulate changes in the thermal environment according to the cooling strategy. In the first chapter, we describe the development algorithm of 3D-USM and propose an efficient method for calculating key parameters, and simulate the average radiant temperature (MRT), which is an important factor for human thermal comfort, considering complex urban environments.

The second chapter established the effectiveness and reliability of 3D-USM through various field experiments and sensitivity tests, diagnosed the urban thermal environment in representative commercial areas, quantitatively evaluated the cooling effect of street trees and green wall, and presented efficient planting arrangement. As a result of the study, street trees were efficient in planting street trees in consideration of the location of the building and the direction of the road, and green wall was more efficient as it approached the ground level. However, green wall of more than 6 m does not provide a significant cooling effect, emphasizing the need for cost-effective planting location and scale.

The third chapter focused on green roofs to maximize heat reduction effects. Blue green roof is the technology that maximizes environmental benefits by adding a blue retention layer to a green roof, storing rainwater and increasing evapotranspiration. This study focused on evaluating the thermal performance of a blue green roof in the summer and examining its potential for microclimate improvement and energy savings. The individual and interactive effects of the blue green roof elements were evaluated by measuring the upper and lower surface temperatures with incremental application of soil, blue, and green layers and analyzing their synergistic benefits. The results showed that blue green roofs exhibited a cooling effect of up to 7.5 ℃ on the upper surface temperature and up to 17.4 ℃ on the lower surface temperature, showing the greatest potential for improving indoor and outdoor thermal comfort. The synergistic effect of the blue green roof was -0.80 ℃ on the upper and +1.59 ℃ on the lower surface. Our research represents that a blue green roof is innovative to simultaneously counteract a hot environment and result in energy savings, which is essential for sustainable development.

This thesis aims to provide valuable insights into the development of effective urban cooling strategies by developing a 3D-USM and addressing urgent challenges posed by urbanization and climate change. It underscores

the need for detailed considerations of urban environmental conditions to efficiently cool cities. The proposed 3D-USM can accurately and efficiently simulate thermal environments and MRT thermal comfort in complex urban environments using simple input data, guiding the development of efficient cooling strategies for sustainable cities.

Keyword: Microclimate modeling, Urban canopy model, Green infrastructure
Mean radiant temperature, Urban planning, Outdoor environment

Student Number : 2020-38920

Table of Content

List of Figures

List of Tables

I. Introduction

The thermal environment in cities is deteriorating owing to rapid global urbanization (Oke, 1982; Zhao et al., 2014). Increasing impervious surface areas and decreasing green areas are leading to the formation of urban heat islands (UHIs), which refer to the phenomenon of the urban temperature being higher than the surrounding rural temperature (Manoli et al., 2019; Radhi et al., 2013). High urban heat increases the number of heat-related patients and mortalities (Å ström et al., 2011; Sahani et al., 2022; Thorsson et al., 2014). This problem is expected to worsen as climate change continues (IPCC, 2014; Oleson, 2012; Yang et al., 2021).

To effectively reduce excessive heat, it is essential to understand the key factors influencing the Urban Heat Island (UHI) phenomenon. The thermal environment of a city varies owing to various factors, such as climate (Harmay & Choi, 2023; Zhao et al., 2014), urban form (Middel et al., 2014; Yin et al., 2018), city size (Oke, 1973), density (He et al., 2020a, 2020b), surface material (Rajagopal et al., 2023; Rosenfeld et al., 1995). Even under the same climatic conditions, the heat island intensity varies according to the density and morphology of the city (Li et al., 2020). Urban green spaces play an important role in temperature control through decrease in sensible heat that raises temperature by increasing latent heat, and crown shadows reducing the inflow of solar radiation (Armson et al., 2012; Block et al., 2012; Doick & Hutchings, 2013; Konarska et al., 2016).

One of the representative ways to solve the problem of heat island in cities is the cooling effect of trees (Armson et al., 2012; Gunawardena et al., 2017; Konarska et al., 2016). The cooling effect of trees can be distinguished by radiative heat reduction and transpiration (Mirzae and Haghighat, 2010; Rahman et al., 2018). Radiative heat reduction is when the trees reduce the radiant heat reaching the surface of an urban area by blocking or reflecting the radiant heat (Tan et al., 2016; Akbari et al., 2002). It is an effective way to cool the space under the trees by generating shadows (Lin and Lin, 2010). Additionally, the surface temperature of trees can be lower than that of impervious surfaces such as asphalt and concrete, resulting in lower longwave radiation (Taha, 1997), which consequently lowers the temperature. Secondly, transpiration is the process of releasing water absorbed through roots into the atmosphere through the stomata of plant leaves, which reduces the urban sensible heat by increasing the latent heat. These two actions play important roles in relieving urban heat (Wang and Akbari, 2016; Dai et al., 2004; Kim and Coseo, 2018).

“Green roofs” refer to green coverage designed on artificial substrates, which provide multiple environmental benefits through interactions with the microclimate, buildings, and urban ecosystems (Cristiano et al., 2021). These benefits include reduced runoff (Berndtsson et al., 2009), improved air quality (Yang et al., 2008), and increased urban biodiversity (Oberndorfer et al., 2007). From the perspective of thermal performance, green roofs in cities are considered a feasible design strategy for improving urban microclimates and conserving energy (Lin et al., 2013; Virk et al., 2015; Zheng et al., 2021; Ziogou et al., 2018). In particular, buildings play a significant role in greenhouse gas emissions, making efforts to reduce energy consumption essential to creating a more sustainable urban environment. Research is being conducted to find the optimal insulation for reducing energy consumption in buildings (Malka et al., 2022), and green roof is being utilized as a nature-based insulation. The shading provided by the green coverage also reduces the solar heat gain in the building by blocking the solar radiation that penetrates the building (Sailor et al., 2012). The evapotranspiration from the green area increases latent heat, lowering the surface temperature (Cascone et al., 2019; Jim & Tsang, 2011), and thus reduces UHI and the heat energy conducted into the building interior (Imran et al., 2018). In densely populated cities such as Hong Kong and Seoul, which lack green spaces and experience intense UHI effects, green roof can bring considerable benefits (Dong et al., 2020). In particular, the cooling effects of rooftops and pedestrian-level greenery are more pronounced in low-rise buildings (Peng & Jim, 2013).

To effectively achieve urban cooling using green infrastructure, it is necessary to accurately diagnose the thermal environment and predict the effects of green infrastructure. Previous studies have analyzed the thermal environment of cities through remote sensing and situ measurements. Satellite image analysis was used to analyze the wavelength of the surface's response and to grasp the macroscopic thermal environment (Halder et al., 2021; Nichol, 1996). The land surface temperature is an effective indicator for understanding the surface status and evaluating the cooling range and strength according to the urban structure and the size of the green space (Venter et al., 2020; B. Zhou et al., 2017). For example, urban parks over 10 ha have a cooling effect of 1 to 2 ℃ over a distance of 350m (Aram et al., 2019). Measurement using sensors is used to evaluate thermal comfort directly received by humans on a neighborhood scale through atmospheric temperature and radiant heat (Hamdi & Schayes, 2008). Measurements can accurately assess and monitor the thermal status reflecting the surrounding environment (Lin et al., 2012; Rodríguez et al., 2020). However, grasping the comprehensive thermal environment of an urban space is difficult because measurements can be performed in a limited space and time.

Modelling, which explain and predict urban spatial patterns, can be a means of solving the limitations. Modelling can analyze the desired time and space and reflect the changes in spatial heterogeneity (Gál & Kántor, 2020; Meili et al., 2020; Mirzaei et al., 2015; Wang et al., 2021). Through modeling, the effects of climate conditions can be identified and the effects of changes in urban space and urban elements can be predicted, which can be used for urban planning. Gao et al. (2022) quantified cooling effect of park and suggested optimal park area which maximize the effect using Gaussian model. Recently, in order to achieve a sustainable city, an integrated model is being developed in connection with other fields. Meili et al. (2020) presented an urban ecohydrological model that is coupled energy and water balance model by urban green space. Sedaghat & Sharif, (2022) modeled reduction of building energy consumption by vegetation and surface materials with high reflectivity. Modeling can be analyzed under various time and space conditions without limitation and reflect changes in spatial heterogeneity, but verification is required due to the presence of uncertainty. Measurement and modeling can compensate for each other's shortcomings.

As urban spaces are highly diverse, and the effects of green infrastructure vary depending on species, scale, and form, a flexible model that can reflect such complexity is required. A 2D model allows for rapid analysis of urban canyons, which are representative urban spaces, and is effective for simulating spatial patterns with consistent configurations. However, to comprehensively reflect highly diverse urban spaces that vary by region and simulate the cooling effects and thermal environments based on the arrangement and scale of tree planting, green walls, and green roof, a model that takes into account three-dimensional factors is necessary.

Efficient utilization of green infrastructure is crucial. In cities where the urban heat island effect intensifies, maximizing cooling effects using limited space and cost is necessary. To achieve this, strategies that optimize the placement of green infrastructure and maximize its inherent cooling effects can be used. Careful placement of green infrastructure is necessary as the effects it provides vary greatly depending on its placement. The cooling effect of green infrastructure can be achieved through an increase in latent heat flux by evaporation. Therefore, strategies to increase latent heat flux are necessary to maximize the cooling effect.

The purpose of this study is evaluating thermal environment and cooling effect of green infrastructure and suggest strategies to maximize cooling effect. To achieve the purpose, this study is divided into three steps:

1) Developing a 3D urban surface model for accurate thermal evaluation

2) Evaluation of thermal comfort and planting strategy for maximizing cooling effects of urban street trees and green wall

3) Evaluation of Effectiveness of storage system with latent heat flux for maximizing cooling effect of green roof

II. Literature Review

1. Three dimensional heat simulation model

Computational fluid dynamics (CFD) models have been used to investigate and simulate urban microclimate according to urban elements and atmospheric conditions (Blocken, 2015; Toparlar et al., 2017). CFD models, which have the advantage of reflecting 3D urban spaces with a high resolution, was used to predict fluid flows, such as air temperature and wind velocity, by realistically reflecting building form, height-width ratio of the street canyon, surface materials, vegetation patterns (Karimimoshaver et al., 2021; Lin et al., 2008; Okeil, 2010). In a recent study, many studies about urban scale adaptation measures and thermal comfort have conducted using CFD models (Blocken, 2015; Toparlar et al., 2017). However, CFD models are difficult for non-experts to use or apply in large-scale urban models owing to the requirements of high computer performance and computational cost (Mirzaei, 2021; Mirzaei & Haghighat, 2010). In addition, analyzing various greenery strategies repeatedly in complex urban spaces that include terrain, structures, buildings, and meteorological environments requires higher computing power and longer analysis time.

Urban canopy model (UCM) can be an alternative. The UCM is simplified by assuming that the temperature and humidity are constant inside the canopy or by characterizing urban fabric only in average, but the goal is to provide an accurate estimate of the thermal conditions of the urban canopy (Afshari and Ramirez 2021). Although the accuracy of UCM may be somewhat reduced since it does not simulate fluid dynamics, UCM can calculate thermal environments with low computer performance, and its relatively short analysis time allows for repetitive evaluation of various plans, making it a useful simulation model for urban planning. Using simplified two dimensional (2D) archetypal urban canyon representation, UCM describe the impact of urban geometry and its interaction with urban climate (Masson, 2000; Nunez & Oke, 1977; Sabrin et al., 2021; Zhou et al., 2022). Urban modeling systems have captured various urban densities using from simple bulk parameterization to multi-layer urban canopy models based on urban canyons (Chen et al., 2011). Kusaka et al. (2001) proposed a single layer model that assumes infinitely-long street canyons parameterized to represent urban geometry, but recognizes the three-dimensional environment. Martilli et al. (2002) proposed a multi-layer radiation model and re-developed by Park et al. (2018) and Krayenhoff et al. (2020). To reflect the complex urban environment in detail, a limited number of three dimensional (3D) building resolving energy balance models currently exist (Bruse & Fleer, 1998; Kanda et al., 2005; Nice et al., 2018).

	Accuracy	Flexibility	Complexity	Running time	Computer Performance
CFD	○	○	×	×	×
Envi-met	△	△	○	△	△
SOLWEIG	△	×	△	○	○
Rayman	△	×	△	○	○
2D-UCM	△	×	○	○	○

Fig. 1 Previous urban heat simulation model

However, previous models have some limitations to be integrated into the urban planning process of diagnosing current status and comparing various plans. A representative model, RayMan, has a user-friendly interface, but it can calculate at only one point, and it also requires a sky view factor as a difficult input variable, showing low accuracy in complex urban areas (Lee and Mayer 2016; Thorsson et al. 2007). On the other hand, SOLWEIG is accurate, but has the drawback of complex input variables for simulation; direct, diffuse, and global shortwave radiation (Jänicke, Milošević, and Manavvi 2021). Furthermore, both 2D models cannot simulate the effects of green walls by structural limitations.

Envi-met, on the other hand, is a 3D model capable of simulating thermal environments by incorporating complex urban spaces and green infrastructure.

However, it simplifies the latent heat flux resulting from green infrastructure, leading to an underestimation of cooling effects of green wall and green wall.

Therefore, there is a need for a model that can accurately reflect complex 3D urban environments and evaluate the cooling effects of green infrastructure. Additionally, a model that is based on simple input variables, has short simulation times, and does not require high computer performance would be beneficial for non-experts to utilize in urban planning.

2. The cooling effect of green infrastructure

Street trees play a significant role in reducing temperatures and mitigating the urban heat island effect. They provide natural shading and coolness in urban environments. According to a study by McPherson et al. (1997), street trees can lower surface temperatures by an average of 2-9℉ (approximately 1-5℃).

“Green roofs” refer to green coverage designed on artificial substrates, which provide multiple environmental benefits through interactions with the microclimate, buildings, and urban ecosystems (Cristiano et al., 2021). Dong et al. (2020) confirmed that green roofs provide cooling effects within up to

100 m and decrease the average land surface temperature by 0.91 ℃. In experiments conducted in residential areas in Hong Kong, intensive green roofs reduced pedestrian-level air temperatures by 0.5–1.7 °C and showed a maximum effect in low-rise areas (Peng & Jim, 2013). A study conducted in Toronto also reported a 0.4 °C air temperature cooling at the pedestrian level (Berardi, 2016). Lin et al. (2021) found that green roofs play an important role in regulating the thermal environment in areas without large green or water spaces. However, moisture stress caused by shallow soil in cities provides harsh growing conditions for plants, hindering their growth and spread (Benvenuti & Bacci, 2010; Savi et al., 2016).

"Blue-green roofs", which overcome these limitations, combine a blue water retention layer with green roofs. This increases water resource efficiency by storing rainwater and continuously supplying it to the soil and plants, leading to more sustained and larger evapotranspiration (Busker et al., 2022; S. xiao Li et al., 2019). Soil moisture from rainwater storage can effectively reduce heat (Fantozzi et al., 2021). Some previous studies evaluated the thermal performance of green roofs with Blue-Green roof (Nguyen et al. 2022). Shafique et al. experimentally confirmed that blue-green roofs have surface temperatures 5 to 9 °C lower than conventional roofs (Shafique and Kim 2017; Shafique, Kim, and Lee 2016). Recently, a study conducted in Italy found that the average daily temperature is consistently 15 to 20% lower than ambient temperature, and indoor temperatures can be reduced by up to 3.7 ℃ (Cristiano et al. 2022). However, the effects of a combination of green and blue layers have been studied very limitedly to date and are not definitive (Pimentel-Rodrigues and Silva-Afonso 2018). The combination of green roofs and water retention systems has simultaneous effects on indoor and outdoor thermal environments, but the thermal performance mechanisms have not been thoroughly investigated.

III. Scope of study

1. Study process

Firstly, I develop the 3D urban surface model for evaluating thermal environment accurately. Secondly, evaluate cooling effect in pedestrian level according to green infrastructure and propose effective planting strategy of street tree and green wall, after validating proposed model. Lastly, measure cooling effect of Blue-Green roof with synergy.

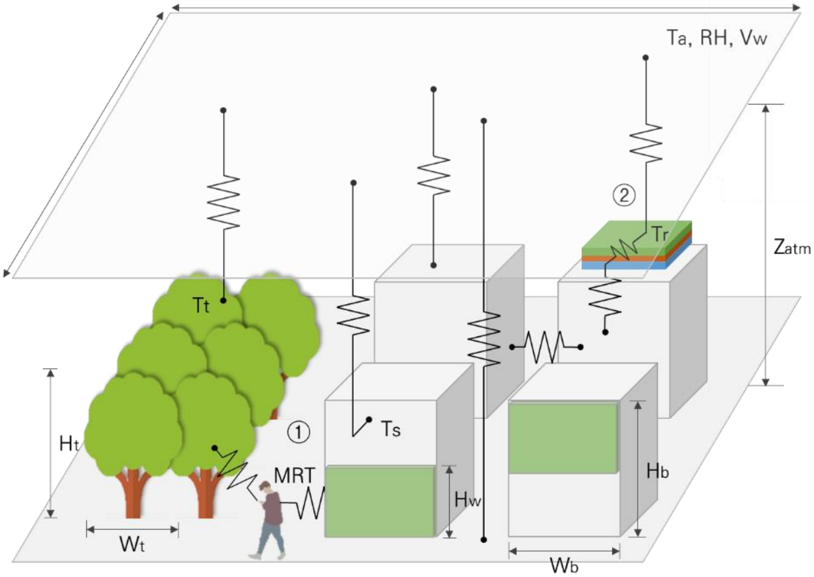

Fig. 2 Study scope

This study evaluated the cooling effect that green infrastructure provides to humans as MRT which is quantity connecting the radiation transfer between the human body and surrounding environment, the cooling effect that provides to the upper and lower spaces of the building, and the thermal performance as the reduced surface temperature.

2. Spatial, temporal scope

The study evaluates thermal environment and cooling effect of green infrastructure. To conduct a detailed evaluation, this study was conducted at a micro-scale in pedestrian level. The thermal performance, which is cooling effect of reduced inner/outer surface temperature, of the green roof is dominant in the roof space of the building, so the cooling strategy research of the green roof for the increase of latent heat flux was conducted at a micro-scale on the rooftop of a single building.

This study focused on evaluating and mitigating urban heat during the summer season, which in Korea falls within the temporal range of June to September. The validation of a 3D urban surface model and the evaluation of thermal comfort based on street orientation were conducted using weather data from June 2018. The overall thermal performance of a green roof system that maximizes the latent heat flux was evaluated from July to September 2022.

IV. Methods

1. Three-dimensional urban surface model

1.1. Model description

The simulation model, which reflects a three dimensional urban space comprises square patches of a certain size, where the patch size is set depending on the analysis resolution, as depicted in Figure 2. Each patch can be set as a different surface, such as cement, concrete, soil, or green.

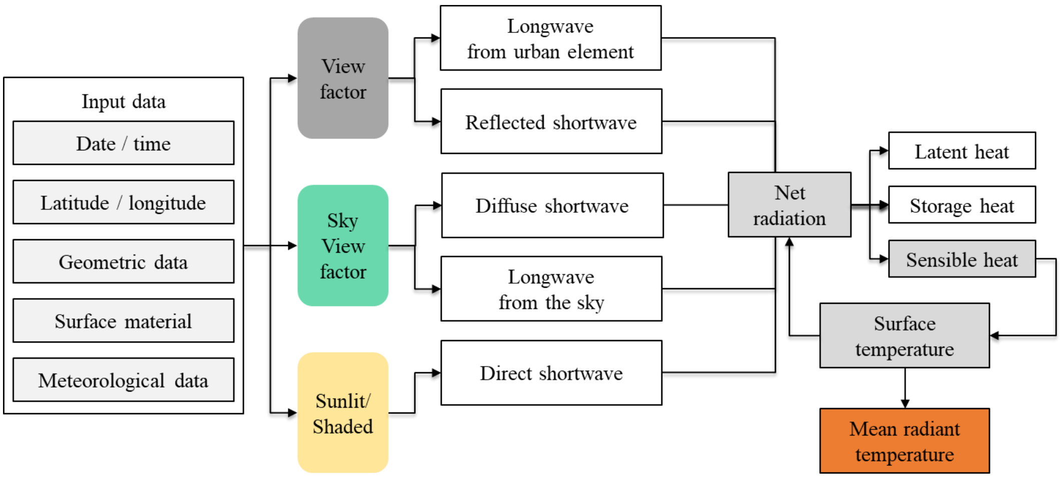

Fig. 3 Model flow for calculating the mean radiant temperature

For calculating MRT, radiative transfer was simulated according to the following input data: date and time, latitude and longitude, geometric data, and meteorological data. Time and location were used to calculate the solar angle and irradiance. Geometric data describing urban structure were used to calculate the three main parameters: view factor, sky view factor, and sunlit/shaded area. Meteorological data, including air temperature, relative humidity, cloud fraction, and wind speed, were used to calculate longwave radiation. Surface material properties used in radiative transfer processes include albedo and emissivity. The model flow for calculating the MRT is depicted in Figure 3.

1.2. Radiative transfer

The net radiation (Rn) of each surface is the sum of the net short and longwave radiation.

$R_n = S \downarrow - S \uparrow + L \downarrow - L \uparrow$ (Eq. 1)

The incoming shortwave radiation is partitioned into direct shortwave radiation (S_{dir}), which is received directly from the sun; diffuse shortwave radiation (S_{dif}), which is received from the sky scattered by the atmosphere; and reflected shortwave radiation, which is reflected by other urban elements (S_{abs}). As each surface reflects incoming shortwave radiation, which depends on its albedo, the net shortwave radiation ($\mathrm{S_{n,i}} = S \downarrow - S \uparrow$) of each surface i can be a function of the albedo and view factor. This model assumed that all surfaces are Lambertian, implying that the reflected or emitted radiation has an equal intensity in all directions. Although rough surface like soil and green may not behave with the Lambertian property (Tu et al. 2017), Lambertian has been assumed in most of urban canopy model for simplifying thermal radiation calculations (Ryu et al., 2016; Wang et al., 2021).

$$S_{n,i} = (1-\alpha_i)(S_{dir,i} + S_{dif,i}) + \sum_{k=1}^{n}\left(\alpha_k(S_{dir,k} + S_{dif,k}) \times VF_{k\to i}\right) \quad \text{(Eq. 2)}$$

where α_i and α_k are the albedo of surfaces i and k, respectively; $VF_{k\to i}$ is the view factor from surface k to i; and n represents all surfaces in the domain. S_{dir} and S_{dif} were calculated using established methods (Allen et al. 1998; Erbs, Klein, and Duffie 1982; Park et al. 2018).

The net longwave radiation ($L_n = L\downarrow - L\uparrow$) of each surface i was calculated using the reflected and emitted longwave radiation from surface i, other urban elements, and the sky using the following equation:

$$L_{n,i} = \varepsilon_i L_{sky,i} - \sigma\varepsilon_i {T_{s,i}}^4 + \sum_{k=1}^{n} VF_{k\to i}\left\{(1-\varepsilon_k)L_{sky,k} + \sigma\varepsilon_k {T_{s,k}}^4\right\} \quad \text{(Eq. 3)}$$

where ε is the emissivity of each surface; $(1-\varepsilon)$ is the reflectivity; $\sigma = 5.67 \times 10^{-8}$ is the Stefan–Boltzmann constant; L_{sky} is calculated as a function of the longwave radiation emitted from the atmosphere using the sky view factor; and T_s is the surface temperature that is dependent on turbulent fluxes, such as sensible heat (H), latent heat (λE), and storage heat (G). This model assumes that latent heat is negligibly low for most urban elements, except green infrastructure. Surface temperature can then be a function of air temperature (T_a), wind speed (v_{wind}), Bowen ratio ($B_0 = 20$), storage heat flux, and net radiation. G was calculated using OHM equations (Grimmond, Cleugh, and Oke 1991).

$$T_s = T_a + \frac{Q-G}{(6.2+4.26v_{wind})(1+{}^{1}/_{B_0})} \quad \text{(Eq. 4)}$$

1.3. Main parameters

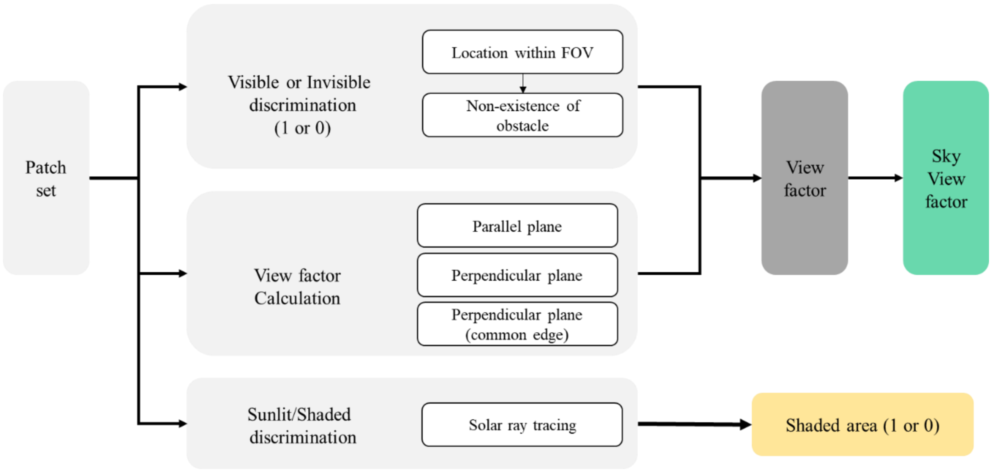

Fig. 4 Algorithm for calculating the three main parameters (view factor, sky view factor, and shaded area)

A key component of the 3D-USM is the calculation of the view factor. The view factor, which is an essential parameter for calculating heat exchange between two objects, means the ratio of the radiation emitted from one patch to another in this model. There are various methods for calculating the view factor. Owing to extremely high computation time required for applying it to a high-resolution 3D space, many studies have simplified the method, which has led to even allowing some error. In the 3D-USM model, analytical and numerical methods, which use the features of the square patch derived from previous studies by Ehlert & Smith (1993), Hottel (1931), Howell (2010), were used to achieve both short computational time and high accuracy.

The process of calculating the view factor consists of two steps (Figure 4): checking whether the two patches are visible to each other and calculating the view factor of the "visible" patches using analytical methods. First, we determined which patches were in a field of view from one patch and then checked whether there were other patches between two patches. In this model, we checked for buildings or other elements as obstacle between all patches.

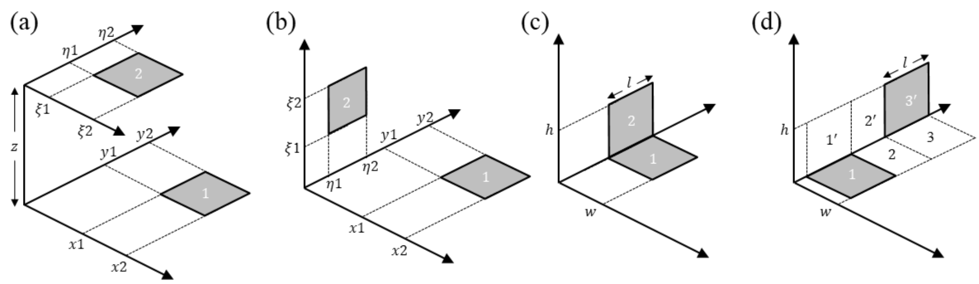

Fig. 5 Four cases of surface relationship for calculating view factors. (a) is parallel plane, (b) is perpendicular plane, and (c) and (d) are perpendicular plane with common edges.

Because 3D-USM consists of square patches, the relationships between all patches have the advantage of being able to be divided into two types: parallel plane (a) and perpendicular plane (Figure 4). Subsequently the perpendicular planes were categorized into three subtypes, namely plane without common edge (b), plane with common edge (c), and plane with a common edge, but not adjacent (d) to ensure the precision of the computations, as illustrated in Figure 4. That is, all two patches were divided into four relationships (a) to (d), and the view factors were calculated using three formulas for each surface relationship using analytic methods (Eqs.5-8). $VF_{m\to n}$ is the view factor from surface m to surface n.

Parallel plane (Ehlert & Smith, 1993) (Eq. 5)

$$VF_{1\to 2} = \frac{1}{(x_2-x_1)(y_2-y_1)} \sum_{l=1}^{2} \sum_{k=1}^{2} \sum_{j=1}^{2} \sum_{i=1}^{2} \left[(-1)^{(i+j+k+l)} G\left(x_i, y_j, \eta_k, \xi_l\right)\right]$$

$$G = \frac{1}{2\pi}\left((y-\eta)[(x-\xi)^2+z^2]^{1/2} \tan^{-1}\left\{\frac{y-\eta}{[(x-\xi)^2+z^2]^{1/2}}\right\} + (x-\xi)[(y-\eta)^2+z^2]^{1/2} \tan^{-1}\left\{\frac{x-\xi}{[(y-\eta)^2+z^2]^{1/2}}\right\}\right) - \frac{z^2}{2}\ln[(x-\xi)^2+(y-\eta)^2+z^2]$$

Perpendicular plane (Ehlert & Smith, 1993) (Eq. 6)

$$VF_{1\to 2} = \frac{1}{(x_2-x_1)(y_2-y_1)} \sum_{l=1}^{2} \sum_{k=1}^{2} \sum_{j=1}^{2} \sum_{i=1}^{2} \left[(-1)^{(i+j+k+l)} G\left(x_i, y_j, \eta_k, \xi_l\right)\right]$$

$$G = \frac{1}{2\pi}\Big\{(y-\eta)(x^2+\xi^2)^{\frac{1}{2}}\tan^{-1}(K)$$

$$-\frac{1}{4}(x^2+\xi^2)(1-K^2)\ln[(x^2+\xi^2)(1+K^2)]\Big\}$$

where $K \equiv (y-\eta)/(x^2+\xi^2)^{1/2}$.

Perpendicular plane with common edge (Hottel, 1931),

$$VF_{1\to 2} = \frac{1}{W\pi}\Bigg(W\tan^{-1}\frac{1}{W} + H\tan^{-1}\frac{1}{H} - \sqrt{W^2+H^2}\tan^{-1}\sqrt{\frac{1}{W^2+H^2}} +$$

$$\frac{1}{4}ln\left\{\frac{(1+W^2)(1+H^2)}{1+W^2+H^2}\left[\frac{W^2(1+W^2+H^2)}{(1+W^2)(W^2+H^2)}\right]^{W^2}\left[\frac{H^2(1+W^2+H^2)}{(1+H^2)(W^2+H^2)}\right]^{H^2}\right\}\Bigg) \quad \text{(Eq. 7)}$$

where $\mathrm{H} = \mathrm{h/l}$ and $\mathrm{W} = \mathrm{w/l}$.

The view factor for the perpendicular plane with a common edge, but not adjacent (d), was calculated using Eq. (8) obtained from the study by Narayana (1998):

$$VF_{1\to 3'} = \frac{1}{2}\left({VF_{123\to 1'2'3'}}^2 + {VF_{2\to 2'}}^2 - {VF_{12\to 1'2'}}^2 - {VF_{23\to 2'3'}}^2\right) \text{ (Eq. 8)}$$

The sky view represents the ratio at a point in space between the visible sky and a hemisphere centered over the analyzed location (Oke, 1982) and was calculated by subtracting the sum of the view factors from one patch to all other patches from

$$\mathrm{SVF}_i = 1 - \sum_{k=1}^{n} VF_{i\to k} \text{ (Eq. 9)}$$

The sunlit/shaded area is determined by launching collimated rays from each surface toward the sun and testing whether the rays are blocked by urban structures. The ray direction is defined by the local solar azimuth and zenith angles calculated using data, time, latitude, and longitude.

1.4. Energy balance of leaf

Energy budget for a leaf consist of sensible heat and latent heat.

$$R_{net} = H + \lambda E = \rho_a C_p \frac{(T_s - T_a)}{r_a + r_b} + \frac{\rho_a C_p}{\gamma} \frac{(e_{sat}(T_s) - e_a)}{r_a + r_b + r_s} \quad \text{(Eq. 10)}$$

where p_a (kgm^{-3}) is the air density, which can be calculated usi ng the ideal gas law, expressed as a function of air temperature and atmospheric pressure P_{atm} (Pa), $C_p = 1005$ $(\mathrm{J\ kg^{-1}K^{-1}})$ is the specific heat of air at constant pressure, and e_a is the air vapor pressure calculated using saturation vapor pressure e_{sat} and relative humidity RH (%). The saturation vapor pressure is calculated from the Arden-Buck equation (Buck 1981, 2012). γ $(\mathrm{Pa\ K^{-1}})$ is a psychrometric constant, and Eq. (11) is generally used (Loescher et al., 2009).

$$\gamma = \frac{C_p P_{atm}}{\varepsilon \lambda} \quad \text{(Eq. 11)}$$

where $\varepsilon = 0.622$ $(-)$ is the ratio of molecular weight of water vapor/dry air, and $\lambda = 1000(2501.3 - 2.351 * T_a)$ (J kg^{-1}) is the latent heat of water vaporization.

r_a, r_b, and r_s (sm^{-1}) are the aerodynamic resistance, leaf boundar y resistance, and stomatal resistance, respectively. Three resistance are the main parameter for leaf energy budget and leaf surface temperatur e. However, because the surface temperature didn't exist at first, 3D-USM assumed that the surface temperature of the leaf was equal to t he air temperature and found the converging value by repeating the e nergy budget simulation.

1.4.1. Leaf boundary resistance

The leaf boundary layer resistance is calculated from the mean plant leaf boundary conductance g_b (ms^{-1}), which is a function of wind speed and therefore of height within the canopy, using Eqs. (12-13) from Jones (1983) and used by Choudhury and Monteith (1988) and Shuttleworth and Gurney (1990).

$r_b = 1/g_b$ (Eq. 12)

$g_b = a\left(u(H_k)/d_{leaf}\right)^{1/2}$ (Eq.13)

where $a = 0.01$ $(ms^{-1/2})$ is an empirical coefficient [46], d_{leaf} (m) is the characteristic leaf dimension, often referred to as the leaf width, and

$u(H_k)$ (ms^{-1}) is the wind speed at each layer height H_k. The wind speed profile is assumed to be logarithmic above the urban canopy and exponential within the urban canyon using Eqs. (14-15) (Mahat, Tarboton, and Molotch 2013; Masson 2000).

$$u_{H_c} = u_a \frac{\ln\left(\frac{H_c - d_0}{z_o}\right)}{\ln\left(\frac{z_{atm} - d_0}{z_o}\right)} \text{ (Eq. 14)}$$

$$u_{H_k} = u_{H_c} \exp\left(-\beta\left(1 - \frac{H_k}{H_c}\right)\right) \text{ (Eq. 15)}$$

where u_a (ms^{-1}) is the wind speed at reference height, and β $(-)$ is the light extinction parameter, which is calculated from Wright (1965); d_0 (m) and z_o (m) are the zero displacement height and aerodynamic roughness length, respectively, which are calculated according to the approach developed by Macdonald et al. (1998) and modified by Kent et al. (2017) as follows, using Eqs. (16-17):

$$d_0 = \left(1 - \alpha_{\mathrm{A}}^{-\lambda^p}(\lambda^p - 1)\right) H_c \text{ (Eq. 16)}$$

$$z_o = H_c\left(1 - \frac{d_0}{H_c}\right) \exp\left[-\left(\frac{1}{k^2} 0.5\beta_A C_{Db}\left(1 - \frac{d_0}{H_c}\right)\frac{\{A_{f,b} + P_v A_{f,v}\}}{A_{tot}}\right)^{-0.5}\right] \text{ (Eq. 17)}$$

where $k = 0.4$ $(-)$ is the von Karman constant, and $\alpha_{\mathrm{A}} = 0.43$ $(-)$, $\beta_A = 1$ $(-)$, and $C_{Db} = 1.2$ $(-)$ are parameter values for staggered arrays (Macdonald et al. 1998). H_c (m) is the canopy height, λ^p $(-)$ is the plan area index of the urban roughness elements, $A_{f,b}$ (m) is the actual frontal area of buildings, $A_{f,v}$ (m) is the actual frontal area of vegetation, A_{tot} (m) is the total urban plan area, and P_v $(-)$ is the ratio between vegetation drag C_{Dv} and building drag C_{Db}. These parameters were calculated from Guan et al. (2000), Guan et al. (2003), and Kent et al. (2017) using the height of trees and buildings. For volumetric/aerodynamic porosity, the light extinction parameter is calculated as given by Dai et al. (2004), assuming a spherical leaf angle distribution.

1.4.2. Aerodynamic resistance

The aerodynamic resistance is calculated by a simpler method (Fatichi 2010), which assumes a neutral condition as follows using Eqs. (18-19):

$$r_a = \frac{1}{k^2 u_{H_k}} \left[\frac{\ln(z_{atm} - d_0)}{z_o}\right] \left[\frac{\ln(z_{atm} - d_0)}{z_{oh}}\right] \text{ (Eq. 18)}$$

$$z_{oh} = 0.1 z_o \text{ (Eq. 19)}$$

Here, z_{oh} (m) is the roughness length for heat.

1.4.3. Stomatal resistance

As the reciprocal of stomatal conductance is stomatal resistance, stomatal conductance g_s (mol $\mathrm{m^{-2}s^{-1}}$) is calculated first. Many studies have reported that stomatal conductance is closely coupled with leaf photosynthesis (Collatz et al., 1991; Wong et al., 1979). In the proposed model, the stomatal conductance is calculated as a function of leaf photosynthesis A_n (μmol $\mathrm{m^{-2}s^{-1}}$) using Eq. (20) from Ball et al. (1987) used by Baldocchi and Meyers (1998) and Collatz et al. (1991).

$$g_s = \frac{\mathrm{m}A_n hs}{C_s} + g_0 \quad \text{(Eq. 20)}$$

where m $(-)$ is the slope, g_0 (mol $\mathrm{m^{-2}s^{-1}}$) is the zero intercept, and hs and C_s (ppm) are the relative humidity and CO_2 concentration at the leaf surface, respectively. In this model, a modified equation is used from Harley et al. (1992), by using the CO_2 concentration C_a (ppm) and relative humidity rh $(-)$ in the air as follows, using Eq. (21):

$$g_s = \frac{\mathrm{m}A_n rh}{C_a} + g_0 \quad \text{(Eq. 21)}$$

Leaf photosynthesis was simulated according to Farquhar et al. (1980) [60]. The version of the model proposed by Harley et al. (1992) was used, which calculates photosynthesis without including the potential limitation arising from the triose phosphate utilization, and is used by Sinoquet et al. (2001).

$$A_n = \left[1 - \frac{0.5O}{\tau C_i}\right] \min\left(W_c, W_j\right) - R_d \quad \text{(Eq. 22)}$$

where W_c (μmol $\mathrm{m^{-2}s^{-1}}$) is the carboxylation rate when the ribulose bisphosphate (RuBP) is saturated, W_j (μmol $\mathrm{m^{-2}s^{-1}}$) is the carboxylation rate when the RuBP regeneration is limited by the electron transport, τ is the specificity factor for RuBisCO (Jordan and Ogren 1984), R_d (μmol $\mathrm{m^{-2}s^{-1}}$) is the rate of CO_2 evolution in light that results from processes other than photorespiration, and O and C_i (Pa) are the partial pressures of O_2 and CO_2 in the interior leaf, respectively. In the proposed model, $C_i/C_a = 0.7$ is used, where C_a (Pa) is the partial pressure of CO_2 in air typically observed with C3 plants under favorable conditions (Hetherington and Woodward 2003; Prentice et al. 2014; Wong et al. 1979).

W_c obeys competitive Michaelis–Menten kinetics with respect to CO_2 and O_2 as follows, using Eq. (23):

$$W_c = \frac{V_{cmax} C_i}{C_i + K_c\left(1 + \frac{O}{K_o}\right)} \text{ (Eq. 23)}$$

where V_{cmax} (μmol $\mathrm{m^{-2}s^{-1}}$) is the maximum rate of carboxylation, and K_c and K_o (Pa) are the Michaelis constants of RuBisCO for carboxylation and oxygenation, respectively.

W_j is controlled by the rate of electron transport, J (μmol $\mathrm{m^{-2}s^{-1}}$), which depends on PAR. They are calculated as follows, using Eqs. (24):

$$W_j = \frac{\mathrm{J} C_i}{4\left(C_i + \frac{O}{\tau}\right)} \text{ (Eq. 24)}$$

The coefficients for K_c, K_o, R_d, and τ are strong, non-linear functions of temperature (Harley and Tenhunen 1991; Johnson and Thornley 1985). One temperature function used for K_c, K_o, R_d, and τ is given by Eq. (25) from Harley et al. (1992):

$$\mathrm{Parameter}(K_c, K_o, R_d, \tau) = \exp(\mathrm{c} - \Delta\mathrm{H_a}/\mathrm{R}T_{s\prime}) \quad \text{(Eq. 25)}$$

where c $(-)$ is a dimensionless, scaling constant, $\Delta\mathrm{H_a}$ $(\mathrm{J\ mol^{-1}})$ is the activation energy, R $(8.3143\mathrm{JK^{-1}mol^{-1}})$ is the gas constant, and $T_{s\prime}$ (K) is the leaf surface temperature.

The stomatal resistance through the stomatal conductance of Eq. (11) is expressed in biochemical units of $\mathrm{m^2 s\ mol^{-1}}$. The conversion to common units $(\mathrm{s\ m^{-1}})$ for Eq (31) is obtained as follows, using Eq. (26) from Sellers et al. (1996).

$$r_s(sm^{-1}) = \frac{\mathrm{T_f}\ P_{atm}}{0.0224 T_{s\prime}\ P_{atm,0}} r_s(\mathrm{m^2 s\ mol^{-1}}) \quad \text{(Eq. 26)}$$

Here, $\mathrm{T_f} = 273.15$ (K) is the freezing temperature and $P_{atm,0} = 101325$ (Pa) is a reference atmospheric pressure.

$$T_v = \frac{p_a(q_{sat}(T_s) - q_a)}{r_a + r_b + r_s} \quad \text{(Eq. 27)}$$

where q_a $(-)$ is the specific humidity of the air at the reference height z_{atm} (m), $q_{sat}(T_s)$ $(-)$ is the specific humidity at saturation a t the leaf surface temperature.

A complete list of the parameters for calculating resistances is presented in Table 1.

Table 1 Values, units, and sources of the parameters for resistances

Parameter	**Value**	**Unit**	**Source**
m	9.5	–	(Ryu et al. 2016)
g_0	0.081	$\mathrm{molm^{-2}s^{-1}}$	(Harley et al. 1992)
α	0.22	$\mathrm{molmol^{-1}}$	(Ryu et al. 2016)
$c(\mathrm{K}_c)$	35.79	–	(Harley et al. 1992)
$c(\mathrm{K}_o)$	9.59	–	(Harley et al. 1992)
$c(\tau)$	−3.9489	–	(Harley et al. 1992)
$\Delta\mathrm{H_a}(\mathrm{K}_c)$	80.47×10^3	$\mathrm{Jmol^{-1}}$	(Harley et al. 1992)
$\Delta\mathrm{H_a}(\mathrm{K}_o)$	14.51×10^3	$\mathrm{Jmol^{-1}}$	(Harley et al. 1992)
$\Delta\mathrm{H_a}(\tau)$	-28.99×10^3	$\mathrm{Jmol^{-1}}$	(Harley et al. 1992)

1.4.4. Leaf surface temperature

To calculate transpiration and leaf surface temperature simultaneously, the slope of the saturation vapor pressure function Δ (Pa) was used from Campbell and Norman (1998).

$$e_{sat}(T_s) - e_{sat}(T_a) = \Delta(T_s - T_a) \quad \text{(Eq. 28)}$$

$$\Delta = 1000\,\frac{17.502 \times 240.97\ \ e_{sat}(T_a)}{(240.97 + T_a)^2} \quad \text{(Eq. 29)}$$

The latent heat term can be linearized using the saturation vapor pressure function as follows:

$$\lambda E = \frac{\rho_a C_p}{\gamma}\frac{(e_{sat}(T_s) - e_a)}{r_a + r_b + r_s} = \frac{\rho_a C_p}{\gamma(r_a + r_b + r_s)}(e_{sat}(T_s) - e_{sat}(T_a) + e_{sat}(T_a) - e_a) = \frac{\rho_a C_p}{\gamma(r_a + r_b + r_s)}(\Delta(T_s - T_a) + VPD) \quad \text{(Eq. 30)}$$

Using Eq. (10) and (29), Eq. (30) can be written as

$$R_{net} - \rho_a C_p\,\frac{(T_s - T_a)}{r_a + r_b} - \frac{\rho_a C_p}{\gamma(r_a + r_b + r_s)}(\Delta(T_s - T_a) + VPD) = 0 \quad \text{(Eq. 31)}$$

Subsequently, Eq. (31) can be readily solved for the leaf surface temperature to obtain

$$T_s = T_a + \frac{R_{net} - \frac{\rho_a C_p VPD}{\gamma(r_a + r_b + r_s)}}{\rho_a C_p\left(\frac{1}{r_a + r_b} + \frac{\Delta}{\gamma(r_a + r_b + r_s)}\right)} \quad \text{(Eq. 32)}$$

1.4.5. Mean radiant temperature

The MRT is a quantity connecting the radiation transfer between the human body and surrounding environment (ASHRAE, 2013). The MRT is calculated as short and longwave radiation received from the surrounding urban elements for a standing person conceptualized as a rectangular box at a height of 1.5 m (Höppe, 1999) using the MRT equation Eq. (10). The six-directional radiation method, which is a representative and accurate measurement method for measuring and calculating outdoor MRT, was used (Du et al. 2020; Thorsson et al. 2007). After simulating the short and longwave radiation received by the six sides of the box (p_i), the radiation term was weighted using the respective share of the surface facing a given direction (w_i=0.06 and 0.22 are vertical and horizontal surface fractions, respectively).

$$MRT = \left[\sum_{i=1}^{6}\left[w_i \frac{1}{\sigma}\left\{\sum_{k=1}^{n} VF_{k\rightarrow p_i}\left(L\downarrow + \varepsilon_k \frac{K_{dif}+K_{ref}}{\varepsilon_p}\right) + \varepsilon_k \frac{K_{dir}}{\varepsilon_p}\right\}\right]\right]^{0.25} - 273.15 \quad \text{(Eq. 33)}$$

where i is the six side of the box; ε_k is the absorption coefficient, and ε_p is the emissivity of the pedestrian, which has standard values of 0.7 and 0.97 (Lindberg and Grimmond 2011).

2. Model validation and application

2.1. Validation

2.1.1. Radiation with sky view factor

3D-USM has the advantage of accurately calculating the view factor and the sky view factor with a simple algorithm by configuring the city's three-dimensional space as a square grid and dividing all plane relationships into vertical and parallel relationships. The performance of the model was verified in the mid-rise residential area (Daehak-dong, Gwanak-gu, Seoul), targeting the sky view factor. The sky was distinguished from the photograph measured by the fisheye lens and compared with the simulated value of the model.

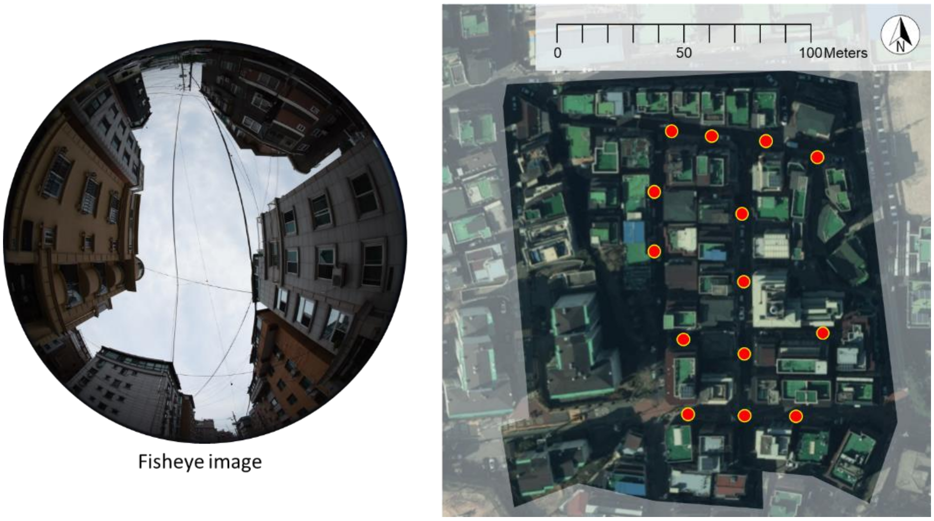

Fig. 6 Validation site for sky view factor

The validation of the model targeting radiation transfer was conducted in the high-rise commercial area (Yeoidong, Yongdeungpo-gu, Seoul) and mid-rise residential area (Daehak-dong, Gwanak-gu, Seoul), targeting the sky view factor. The incident radiation from the upper side was compared with the measured value of the week (0900 LST – 1800 LST) and the simulation value. At each site, CNR4 Net Radiometer (Kipp & Zonen, Netherlands) with a sensitivity 5 – 20 $\mu V/W/m^2$ was used to measure the short and longwave radiation.

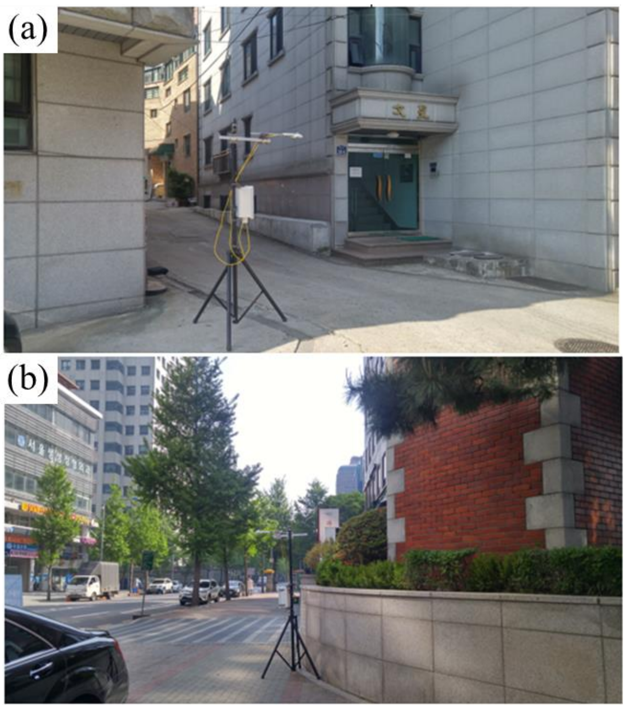

Fig. 7 Validation site for radiation (a) High-rise commercial area, (b) Mid-rise residential area

2.1.2. Surface temperature

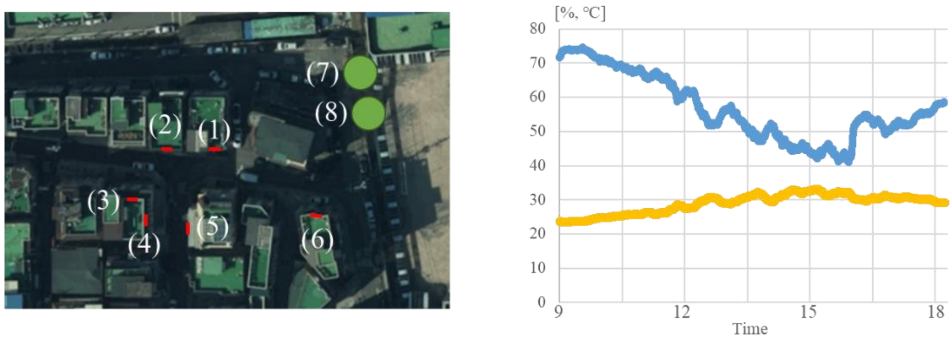

Fig. 8 Validation site for surface temperature.

The validation of the model targeting surface temperature was conducted in the mid-rise residential area (Daehak-dong, Gwanak-gu, Seoul. The surface temperature was measured at 6 points of building wall and 2 points of street trees; Zelkova serrata (Thunb.) Makino, every 30 minutes during the day from 0900 LST to 1800 LST on June 23, 2023. Surface temperature is measured by a handheld Fluke Ti100 thermal camera (Fluke Systems, USA). The data have an approx. spatial resolution of 0.06 m and a footprint of 0.006 ha and albedo from CNR4. Meteorological data including air temperature, relative humidity, and wind speed are measured at 10-second intervals using the Onset Hobo S-THB-M002, S-WCF-M003 and logged by the Hobo station (Bourne, MA, USA). I estimated the key photosynthetic parameters, Vcmax and Jmax, from leaf gas exchange measurements using a portable photosynthesis system

(Li-6400); Li-Cor Inc., Lincoln, NE, USA). Vcmax and Jmax area the maximum rates of carboxylation and electron transport, respectively. First, the photosynthesis rate (A) responding to leaf internal CO2 concentrations (Ci) were measured to obtain A/Ci curves. For each leaf, the automated program mode in Li-6400 to create an A/Ci curve was used by changing leaf external CO2concentrations (400, 200, 50, 100, 200... 1400 ppm). Second, Vcmax and Jmax from the obtained A/Ci curves we were estimated using a least-squares curve-fitting method to fit the measured A/Ci curve to the FvCB model. And Vcmax and Jmax were estimated using the Microsoft Excel^{TM} spreadsheet provided by Sharkey et al. (2007).

2.1.3. MRT with Sunlit/Shaded area

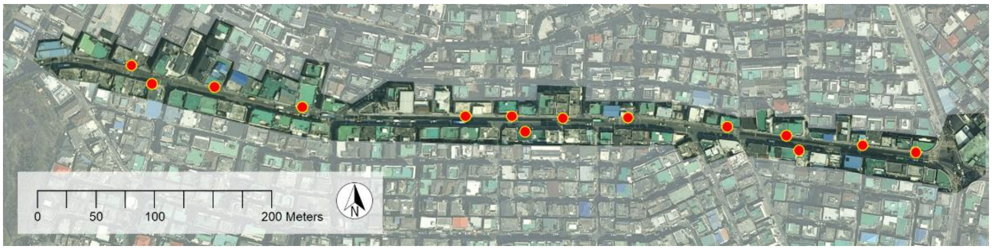

Fig. 9 Validation site. MRTs were measured at 14 points (red points)

Sunlit/Shaded areas are very important parameters for urban thermal environments because they determine the presence or absence of shortwave radiation from the sun. The study area is E–W Street without trees, a mid-rise commercial area in a high-density city (Jangwi-dong, Seongbuk-gu, Seoul). Shadow was calculated with 3D-USM at an hour interval during the summer of June to August in Korea and compared with the simulation results using Hillshade, ArcGIS shadow calculation algorithm.

This area is E–W Street which has been considered thermally uncomfortable in comparison to the S–N one. The E-W Street consists of three streets of similar patterns (Street 1, 2, 3) with different rotational angles (12.5°, 0°, and 6.5°) due to two bends, and is an urban canyon of a fixed width without trees. To validate the model performance, MRTs were measured at 3-4 points to the north which is sensitive to the length and direction of the shadow, 1 point to the south, a total of 14 points (Figure 9a). At each point, CNR4 Net Radiometer was used to measure the short and longwave radiation in six directions (front, rear, upper, lower, left, and right) for approximately 5 min, and the average MRT values of each point were calculated using Eq. (10). The MRTs were measured every 1 second for 5 minutes and controlling the surrounding environment within 2m to minimize errors caused by changes in the surrounding environment, such as human and vehicle movements. Meteorological data including air temperature, relative humidity, and wind speed are measured at 10-second intervals using the Onset Hobo S-THB-M002, S-WCF-M003 and logged by the Hobo station (Bourne, MA, USA).

The accuracy is 0.21℃ for temperature, 2.5% for relative humidity, and 1.1m/sec for wind speed. The measurement was measured from 1400 LST to 1600 LST on June 20, 2018, and geographic data, including the height of the surrounding building, road length, width, and height of trees, were inputted for simulation. The commonly used strategies for model validation are statistical analysis and trends comparison (Fabbri & Costanzo, 2020), and this study utilized the former approach. The statistical analysis of measured and simulated MRT involved the calculation of the coefficient of determination (R2), the Root Mean Square Error (RMSE), and the Mean Absolute Error (MAE).

2.2. Simulation

Fig. 10 Three streets distinguished by the angle of rotation. Red dashed line is northern sidewalk and blue dashed line southern sidewalks

After model validation, this study focused on difference of thermal comfort at pedestrian level from changes in the angle of the sidewalk. The detailed environmental changes of the E–W street were assessed using MRT analysis, by dividing the E–W road into three streets according to the rotation angles (12.5°, 0°, and 6.5°, Figure 10). The change in thermal comfort that a person feels while walking on a real road along the two sidewalks in the north and south was analyzed linearly and not in points. It was analyzed at 1300 LST, when the sun was at the highest altitude and solar radiation had the highest value, 0900 LST, and 1600 LST, which had the same azimuth difference (approximately ±90 °) and same altitude (approximately 43°) from the north (180°).

Table 2 Meteorological data for simulation

Input data	0900 LST	1300 LST	1600 LST	Units
Air temperature	22.8	25.1	26.6	℃
Relative humidity	77.1	66.2	61.5	%
Wind speed	1.2	1.2	2.2	*m/s*

2.3. Green infrastructure scenario

2.3.1. Street tree

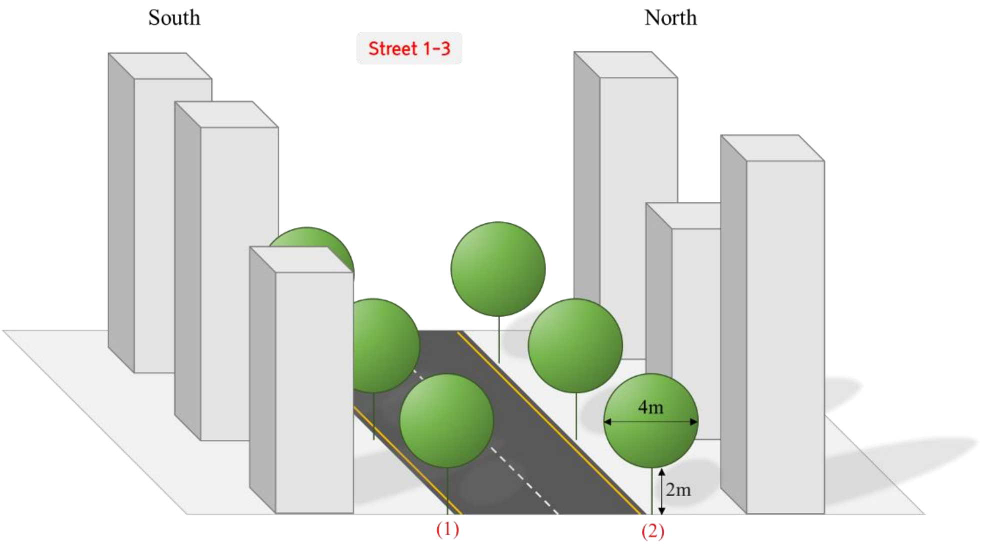

Fig. 11 Street tree planting scenario. Trees are planted at southern (1) northern side (2)

To analyze the cooling effect of trees that varies according to the change in the detailed angle of the road, a simulations of the cooling effect were performed by two planting scenarios (Figure 11). For the planting simulation, the shape of the trees was set to spherical, the height of the underground to 2 m, the width of the crown to 4 m, albedo to 0.3, and the leaf area density to 0.5. The decrease in shortwave radiation due to the shadow of the tree crown and its transmittance were calculated using the method proposed by Welles

& Cohen (1996), which takes into account the zenith angle of incidence of the radiation and the fraction of leaf area.

2.3.2. Green wall

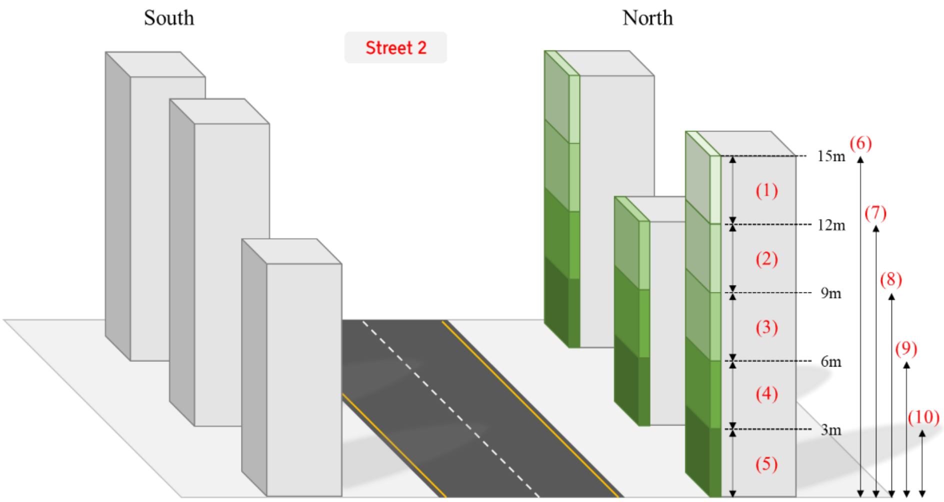

Fig. 12 Green wall planting scenario. The number shows each planting area.

Green wall installed on artificial ground has the effect of improving the thermal comfort of pedestrians unlike green roof. First, in order to evaluate the cooling effect according to the location, green wall of the same area was set according to the height and simulated and compared (Figure 12, 1-5). Since the building of the target site is up to 15m, green wall was installed at intervals of 3m. Second, in order to evaluate the cooling effect according to the area, the height of green wall from the ground was installed differently and simulated and compared (Figure 12, 6 – 10). For simulation, albedo was set to 0.3 and leaf area density was set to 0.5.

3. Evaluation of Effectiveness of storage system with latent heat flux for maximizing thermal performance of green roof

This study focuses on the thermal performance and mechanisms of blue-green roofs. First, to investigate the differences in thermal performance according to the step-by-step application of the soil layer, blue retention layer, and greening layer from the gray roof, measurement experiment was designed. Secondly, statistical analysis was used to evaluate the thermal performance and synergy according to the type of roof and to analyze the causes. Lastly, based on the thermal performance of blue-green roofs, the effects on outdoor and indoor spaces and other environmental benefits were discussed.

3.1. Climate conditions

The study site was located on top of a Seoul National University building in Seoul, South Korea, which is geographically located in the temperate climate zone of the mid-latitudes; therefore, the four seasons of spring, summer, fall, and winter are clearly distinguishable. The summer (July to September) is characterized by hot weather due to high temperatures and humid North Pacific high pressures.

Table 3 Climatic data of Seoul, South Korea (2022)

Input data	July	August	September	Units
Monthly average daily temperature	27.3	25.7	22.4	℃
Maximum monthly average daily temperature	31.0	28.9	27.2	℃
Minimum monthly Average daily temperature	24.2	23.1	18.2	*℃*
Average monthly daily rainfall	8.13	18.22	6.72	*mm/days*
Number of Rainy Days	14	19	8	*days*

3.2. Experimental set-up

The experimental group consisted of five roofs: a module with only a soil layer (Soil), a module with a blue retention layer (Blue), a planting module

(Green), and a planting module with a blue retention layer (Blue-Green). A conventional roof (Gray) was set as the control group. The modules of the experimental group were 50 x 50 cm squares and consisted of a 20 cm soil layer composed of bottom ash-based lightweight soil, a 10 cm blue retention layer, and an intermediate plate for separation from the soil layer. To supply stored water to the soil layer, the lower end of the middle plate was cone-shaped with a small hole so that the absorbed water was delivered to the upper layer. The plant used in the experiment was Sedum takesimense Nakai, which is mainly used as a material for low-management and lightweight green roof, and highly adaptable to barren environments (Li & Kang, 2013). The measurement experiment was conducted at a distance of approximately 5 m or more from other structures and was not affected by shadows considering the direction of the sun.

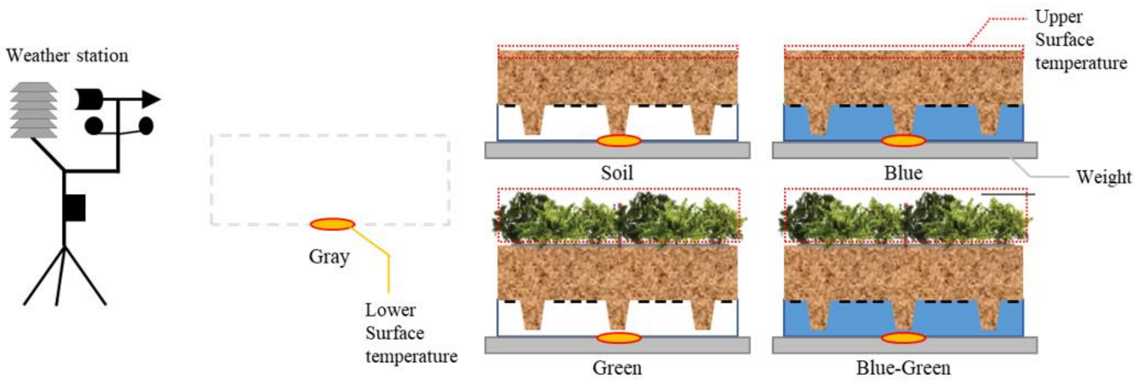

Fig. 13 Schematic cross-section of the studied roof types with sensors for environmental monitoring. Roof types included a soil layer (Soil), a module with a blue

retention layer (Blue), a planting module (Green), a planting module with a blue retention layer (Blue-Green), and a conventional roof (Gray) as the control.

3.3. Measurements

The experiment was conducted from July 14 to September 30, 2022 on the roof of a building on the Seoul National University campus. To evaluate the thermal performance of blue-green roofs, the surface temperatures at the top and bottom of each of the five roofs were measured. The upper surface temperatures of the roof modules, including the roof, were measured every 30 seconds using a COX CG-640 longwave infrared (LWIR) camera with a video resolution of 640 × 480 pixels and 30 Hz video sampling. The spectral range of the camera was 8–14 μm, and the surface temperatures had an accuracy of ± 2 %. The lower surface temperatures were measured every 10 seconds using resistance of thermal detector (RTD) sensors that were connected to data logging temperature recorders with an estimated system accuracy of 0.15 ℃. The sensors were attached to the floor surface, which was approximately 3 cm from the center of each module. The evapotranspiration of plants and soil was measured at a 1-second interval using an SB-100K electronic balance with a capacity of 100 kg and a resolution of 1/6000. All data were analyzed by averaging at 1-minute intervals. Albedo (i.e., the ratio of incoming and outgoing shortwave radiation) was measured using a net radiometer (CNR4, Kipp & Zonen, NL) above the gray roof, soil, and greenery. Air temperature and relative humidity were measured at 10-second intervals using the Onset Hobo S-THB-M002 and logged by the Hobo station (Bourne, MA, USA). The data were then averaged at 1-minute intervals.

Fig. 14 Experimental site. The five roof types and the surrounding experimental set-up including the equipment for measuring the environmental parameters.

3.4. Statistical analysis

R version 3.3.3 was used for statistical analyses. To investigate the difference in temperature reduction between the modules, we conducted an ANOVA test, excluding rainy days. Normality of the distribution was checked qualitatively using quantile plot (QQ-plot) and formally with a Shapiro-Wilk test, which confirmed the non-normality of some variables. Nevertheless, when the group size is the same, the F-statistics are quite robust to violations of normality, as is the case with the data in this study (Field, 2009). Also, if the sample size is large enough, test is relatively robust to moderate violations of the normality assumption (Lumley et al. 2002; Sawilowsky and Blair 1992). Despite showing some deviation from normality assumption in the QQ-plot (Figure A.1), we assumed normal distribution and subjected to Welch's ANOVA with Games-Howell post-hoc tests for quantitative effect evaluation due to the same and large sample size. To understand the relationship between ΔTs (upper and lower surface temperature differences) and time or meteorological data, air temperature, and relative humidity, a Pearson correlation was performed. In all cases, the means were reported to be significant when $p < 0.05$.

3.5. Heat balance

Green roof provides cooling effects through the process of evapotranspiration, and this effect is expected to be amplified when combined with a retention tank. This significantly contributes to the energy balance of green roofs. Thus, qualitative energy estimates related to evapotranspiration were performed. Daily evapotranspiration was estimated by measuring the weight change of the module over one sunny day without rain. The latent heat (LE) caused by the evapotranspiration (ET) in the greening module can be expressed as follows (Refahi & Talkhabi, 2015):

$$LE = \lambda \times ET \quad \text{(Eq. 34)}$$

where λ represents the latent heat of evaporation (2422 kJ/kg at 35 ℃). The latent heat was compared with solar radiation, which is the main load on the heat balance in summer. The daily amount of accumulated solar radiation was obtained from an automatic weather station near the experimental site. Using the albedo measured according to the surface material (Roof, Soil, and Green), the reflected solar radiation was calculated and the solar energy balance was analyzed according to the roof type by modified version of the equation excluding longwave radiation as follows (Grimmond and Oke 1999):

Incident solar radiation = Reflected heat + Latent heat + Sensible heat + Storage heat (Eq. 35)

V. Results

1. Three-dimensional urban surface model

1.1. Model performance

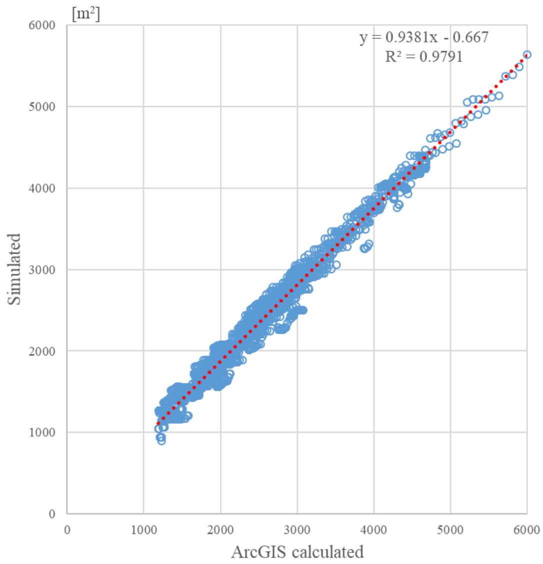

Fig. 15 Sunlit/shaded algorithm validation

As a result of calculating the shadow for the summer three-month period using ArcGIS and comparing it with the simulated result, it was found that the sunlit/shaded algorithm of 3D-USM in the three-dimensional space simulates the shadow well (Figure 15).

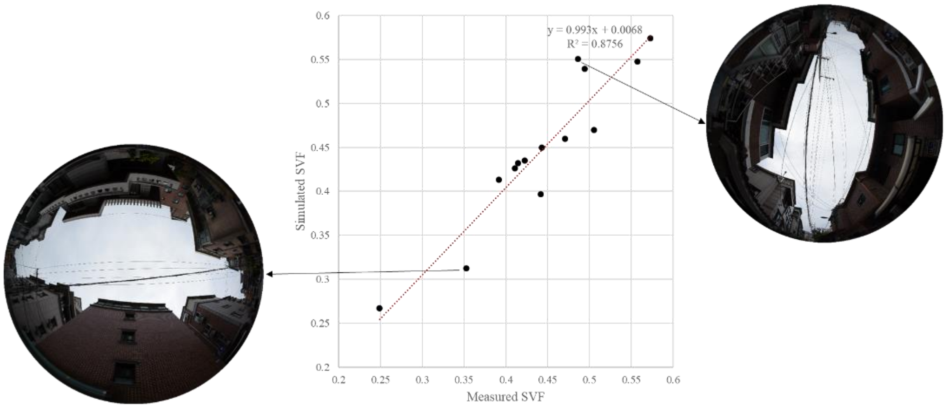

Fig. 16 Validation of sky view factor. The two pictures of the fisheye lens show the cause of the error caused by the uneven shape of the building.

According to the statistical analysis, the measured and simulated SVF showed a high R^2 value of 0.87 and a positive correlation within the study area. The shape of buildings often has a polygonal shape different from that of maps. It is judged that the error of the model for SVF simulation increases when its shape is significantly different from that of the map (Figure 16).

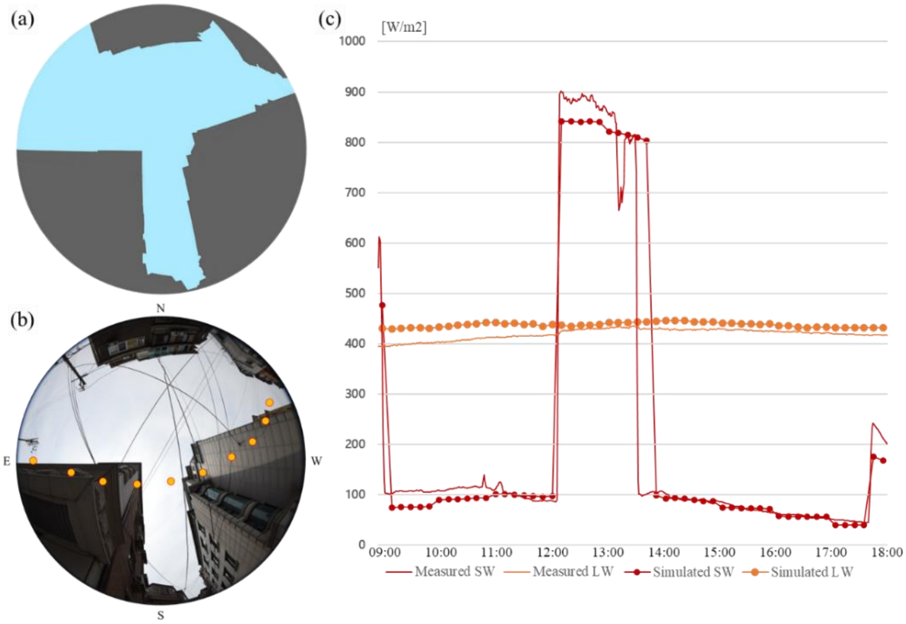

Fig. 17 Measured data in mid-rise residential area at 1 June, 2018. (a) Sky view from fisheye lens (b) Solar path from 0900 LST to 1800 LST (c) Measured and simulated Short and Longwave radiation

In the simulation conducted on the Mid-rise residential area, SVF was calculated to be 0.5472, slightly lower than the measured value of 0.5579. As a result, scattered short waves from the sky would have been underestimated in the model, and long waves from surrounding buildings with surface temperatures relatively higher than atmospheric temperatures would have been overestimated (Figure 17). This pattern was similar in the high-rise commercial area (Figure 18). The simulated SVF was calculated to be 0.5674, lower than the measured value of 0.6122, and as a result of the radiant heat simulation, the short wave was calculated to be smaller and the long wave was calculated to be larger. SVF's underestimation is believed to have occurred because it reflects the shape of the building in the form of a rectangular parallelepiped, and indicates that the more complex the building is, the greater the error may be.

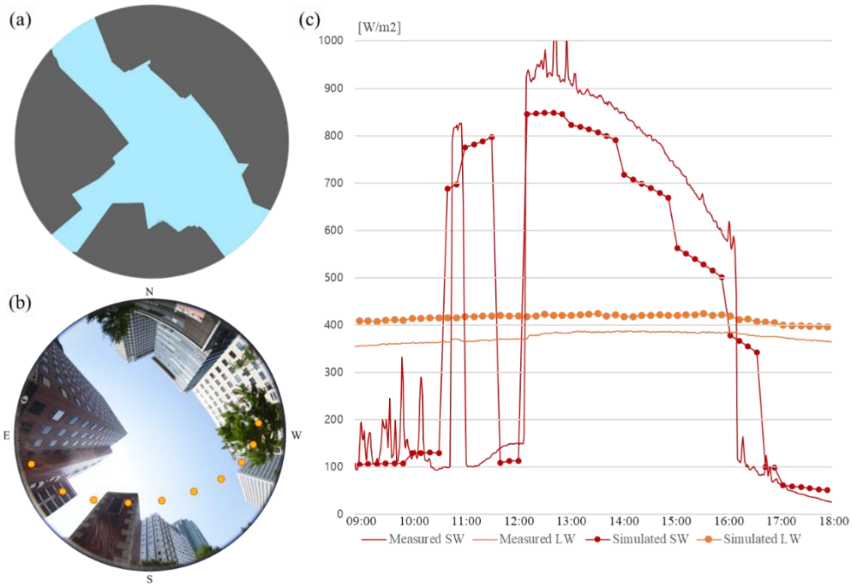

Fig. 18 Measured data in high-rise commercial area at 28 April, 2018. (a) Sky view from fisheye lens (b) Solar path from 0900 LST to 1800 LST (c) Measured and simulated Short and Longwave radiation

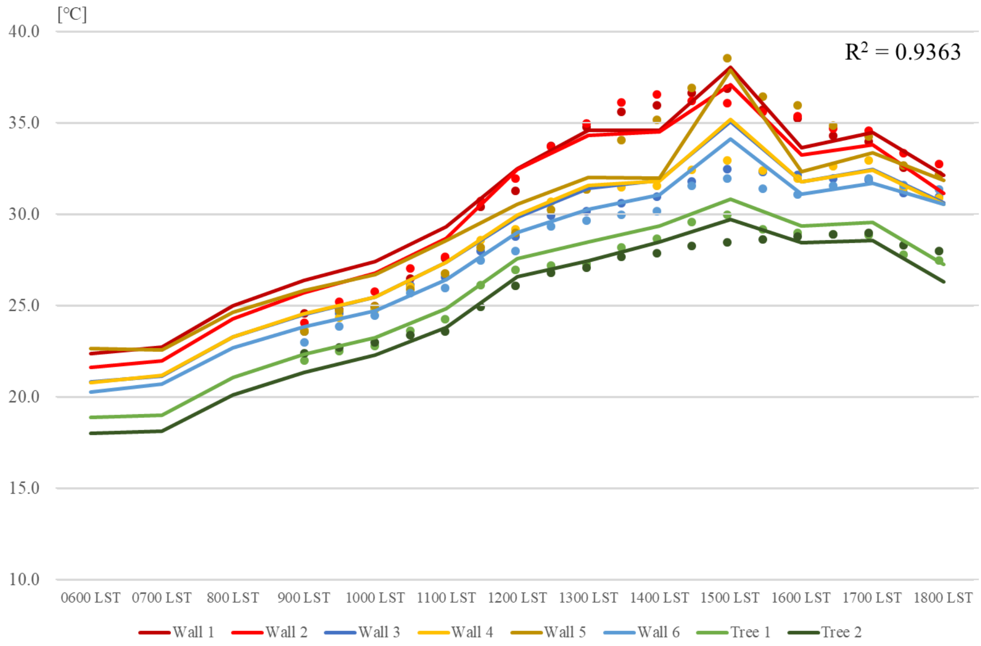

Fig. 19 Validation of surface temperature. Each line shows simulated results and each point shows measured surface temperature.

According to the statistical analysis, the measured and simulated surface temperature showed a high R^2 value of 0.93 and a positive correlation within the study area. Vcmax and Jmax were 52.9 and 65.4 μmol/m^{2}s, respectively. The error appears to have occurred because it was a cloudy day with an average cloudness of more than 0.5.

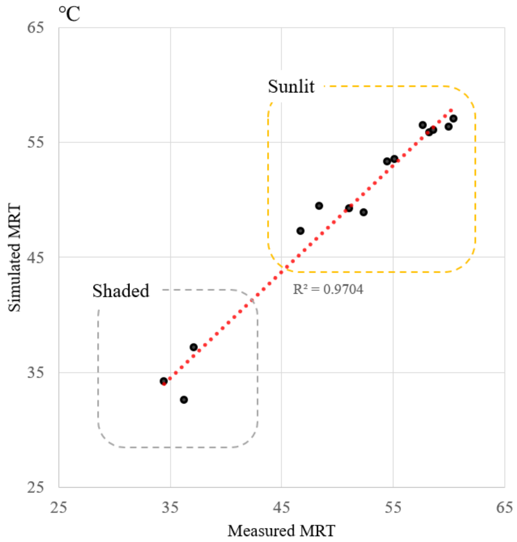

Fig. 20 Model validation results showing estimated MRT in sunlit and shaded areas.

The points in yellow and gray box are estimated in the sunlit and shaded areas, respectively

During the MRT measurement time, the average air temperature was 27.2℃, the relative humidity was 47%, and the amount of solar radiation was 741.3W/m^2, indicating a clear and sunny day. The estimated MRT ranged from 34 to 60℃ (Figure 20).

The measurements were conducted between 1400 and 1600 LST; hence, the three points in the southern were blocked by building shadows, resulting in low MRT values (average 35.9℃). We identified and processed outliers in the data measured at each location during the 5-minute period. The simulation results, with an irradiance of 719.2W/m^2, direct shortwave radiation of

600.6W/m^2, and scattered shortwave radiation of 118.6W/m^2, indicated that the model successfully simulated the decisive impact of shadows on temperature. Other measurement points located in the northern region showed high MRT values (average of 55.0℃) although they were measured in June, which is not as hot as compared to July–August. According to the statistical analysis, the measured and simulated MRT showed a high R^2 value of 0.97 and a positive correlation within the study area. The RMSE (Root Mean Square Error) and MAE (Mean Absolute Error) were 1.43℃ and 1.21℃, respectively, indicating that the model accurately evaluated MRT in study area under conditions with a grid size of 2 m.

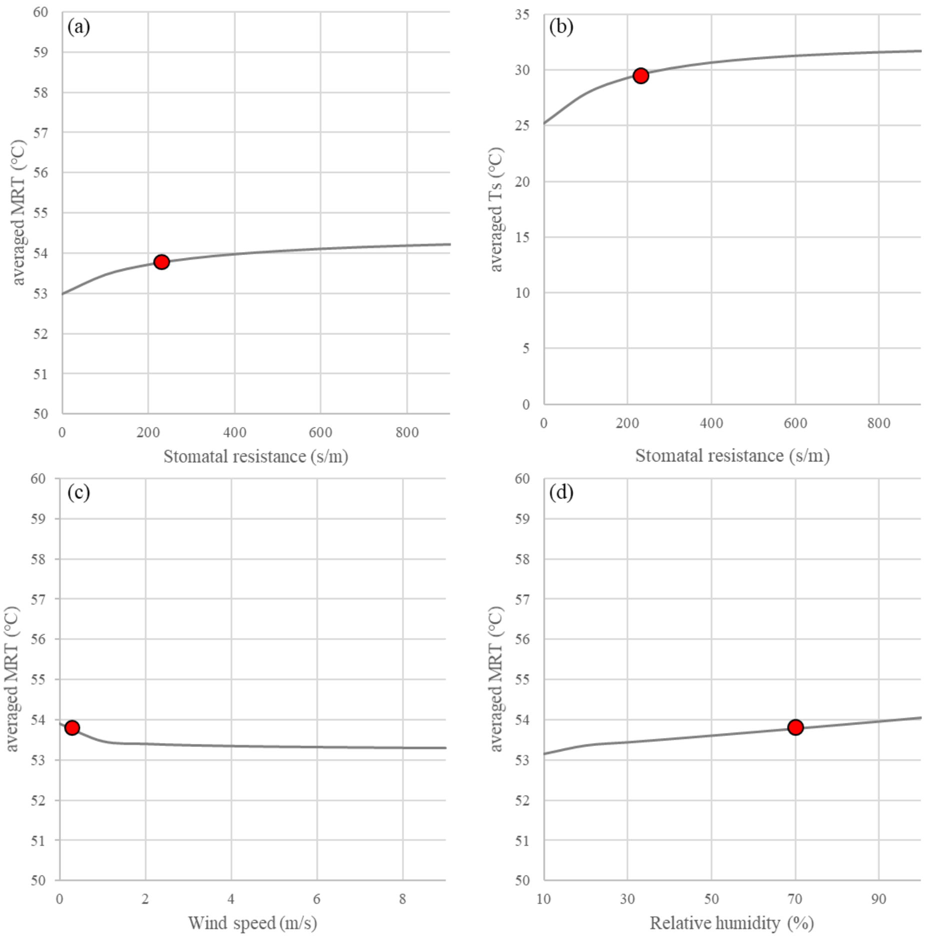

Fig. 21 Sensitivity test of averaged MRT in Street 2 at 1300 LST for (a) stomatal resistance, (c) wind speed, and (c) relative humidity. (b) is sensitivity test of averaged leaf surface temperature for stomatal resistance

In order to calculate the latent heat flux through the transpiration of plants, 3D-USM treated the values of several variables related to pore resistance with a constant based on previous studies. However, there is an error in the thermal environment analysis because it varies depending on the type of plant and the growth environment. In addition, since this model does not reflect fluid dynamics, it cannot reflect microclimate fluctuations such as wind speed and relative humidity inside the space, resulting in errors. As a result of conducting a sensitivity test to identify errors that may occur due to these fluctuations, the change in MRT is about 1 degree (Figure 21), and it is judged that it will not significantly affect the change in MRT according to the angle of the road and the magnitude of MRT reduction due to tree planting (Figure 24, 26). The leaf surface temperature increased significantly from 25.2℃ to a maximum of 31.7℃ as the stomatal resistance changed under the condition of the air temperature of 25.1℃, but MRT was found to have an impact on an increase of up to 1.2℃ (Figure 21 a, b).

1.2. Urban heat simulation

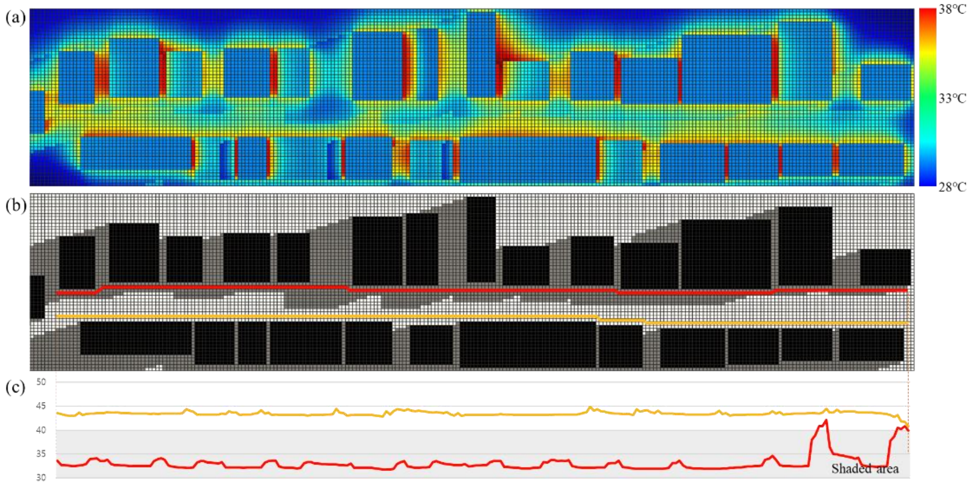

Fig. 22 Model output set. (a) surface temperature, which red represents hot, and blue represents cool surfaces. (b) shaded area, which black indicates building, bright color indicates a high sky view factor, red line represents northern sidewalk, and orange line represents southern sidewalk. (c) MRT at the two sidewalks (0800 LST, Street 1).

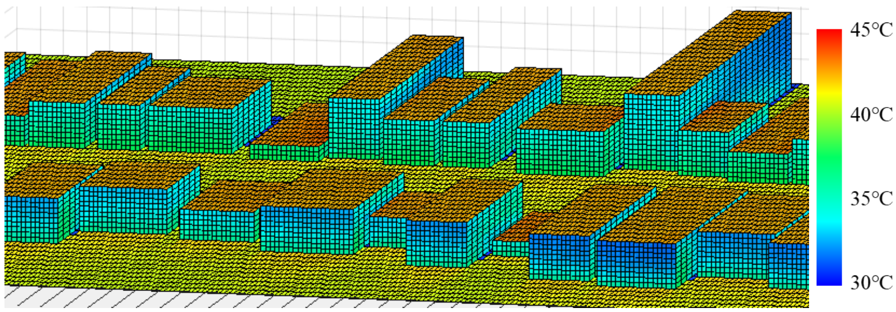

Fig. 23 Three dimensional result of USM (1300 LST, Street 3)

Figure 22 and Figure 23 shows the main result set of the 3D-USM: surface temperature, sunlit/shaded area, and MRT. At 0800 LST, shadows can be seen forming to the west because the sun is in the east (Figure 21b). In contrast to the relatively low surface temperatures on the ground and rooftop caused by the building shadows, the surface temperature in front of the east wall is the highest as it receives high shortwave radiation (Figure 22a). The MRT is determined using long and shortwave radiations received from the surrounding environment and is significantly influenced by direct shortwave radiation owing to the presence or absence of shadows. The MRT (red line) at the pedestrian walking point on the northern sidewalk was significantly lower than that at the pedestrian walking point on the southern sidewalk (orange line) owing to the building shadows, and a slight increase in MRT was observed in the last section where the building shadow disappeared (Figure 22c).

1.3. MRT

MRT simulations showed that MRTs were generally higher in the northern sidewalk (red line) than in the southern sidewalk (orange line) and the highest at 1300 LST for all the streets (Figure 24). The results provide evidence that MRT is predominantly influenced by solar radiation rather than other meteorological conditions. Despite the highest temperature occurring at 1600 LST, the peak of solar radiation was observed at 1300 LST, resulting in the highest MRT value at that time.

Fig. 24 Changes in mean radiant temperature at the sidewalks (red: northern, orange: southern) according to time and street. Ta is air temperature, RH is relative humidity, WS is wind speed, and Rc is solar irradiance

The thermal comfort in the three streets with different angles showed different patterns over time. The MRT of Street 2 with a rotation angle of 0° was similar to that of the two sidewalks at 0900 LST and 1600 LST; in contrast, the MRT of Street 3 with a rotation angle of 6.5° was generally low in the northern sidewalk at 0900 LST and southern sidewalk at 1600 LST. This pattern evidently appeared on Street 1 with a rotation angle of 12.5°, indicating a change in the thermally comfortable sidewalk over time. At 1300 LST, when the sun was at its highest altitude, the MRT was low because of building shadows on the southern walkway in all the streets.

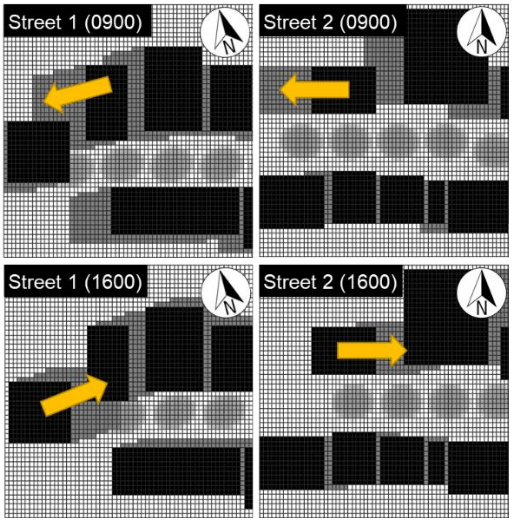

Fig. 25 Different shadow orientations formed according to the rotation angles

The 12.5° street rotation also rotated the shadow's direction by 12.5°, which can have a significant impact on pedestrians walking close to the buildings. As shown in Figure 25, direction of the shadow in Street 2 changes from west to east between 0900 and 1600 LST, which has less impact on pedestrians; however, Street 1 is sensitive to small angular changes because there are ups and downs from southeast to northwest.

1.4. Cooling effect of tree planting scenario

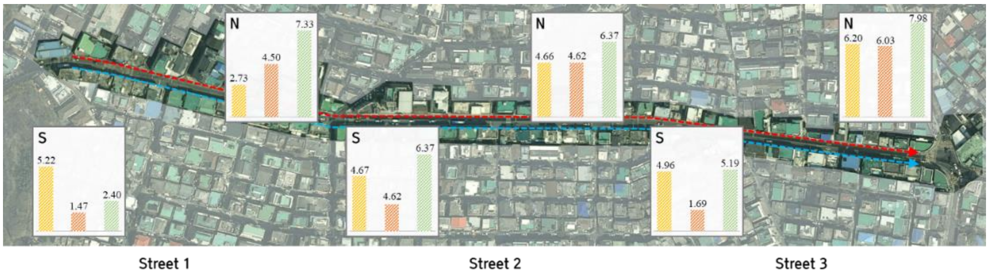

Fig. 26 Changes in average mean radiant temperature with time due to the cooling effect of trees (yellow, orange, and green bars represent 0900, 1300, and 1600 LST, respectively)

Although the trees provided an overall cooling effect in the pedestrians walking spaces, which can be caused by a low surface temperature owing to latent heat, the cooling effect of the trees adjacent to the pedestrian spaces is dominant because of the tree shadows (Figure 26). Overall, the cooling effect of the northern sidewalk was higher than that of the southern sidewalk; however, it was confirmed that the cooling effect received by Street 1 sidewalk varied significantly over time owing to change of shadow direction (Figure 24). This implies that even small variations in the angle of the street can significantly impact thermal comfort over time, resulting in different optimal locations for effective vegetation. Therefore, streets in the same E–W direction need appropriate strategies depending on the its angle.

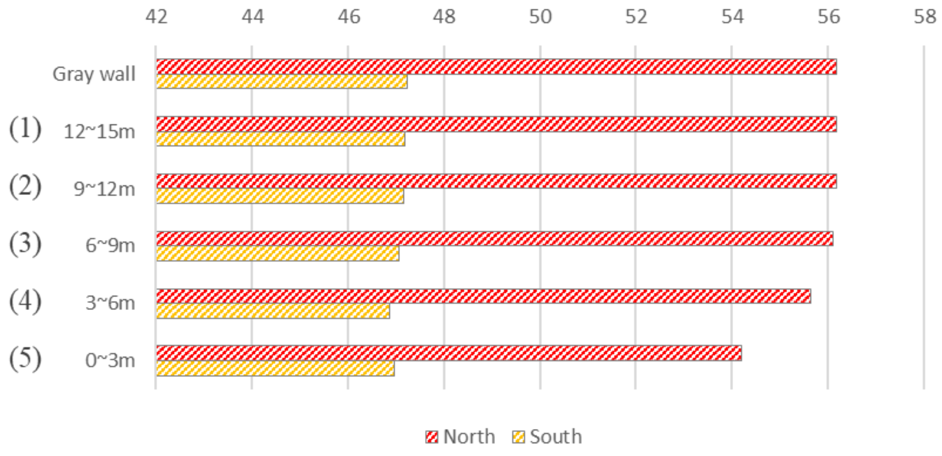

Fig. 27 Mean MRT according to planting height of green wall (Street 2, 1300 LST)

As a result of arranging green wall according to height, the scenario arranged at the bottom significantly reduced MRT in the north (Figure 27). On the contrary, the MRT in the south was effective in a 3-6m scenario, but the reduction effect was not significant due to its long distance. The lower the height, the greater the MRT reduction effect, and the green wall arranged at a height of 6 m or more did not provide a significant effect on the pedestrian-level MRT.

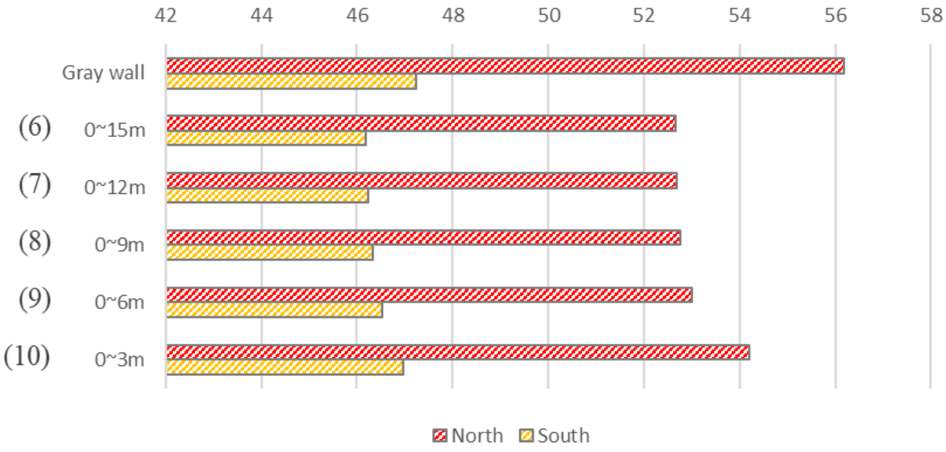

Fig. 28 Mean MRT according to planting area of green wall (Street 2, 1300 LST)

As the high-position green wall is far from the pedestrian and provides a small cooling effect, the required planting area may also vary. Figure 28 shows that the cooling effect decreases significantly as the area of green wall increases, and suggests an efficient planting strategy within a limited budget.

2. Effect of storage system of Blue Green roof for maximizing cooling effect

2.1. Upper surface temperatures

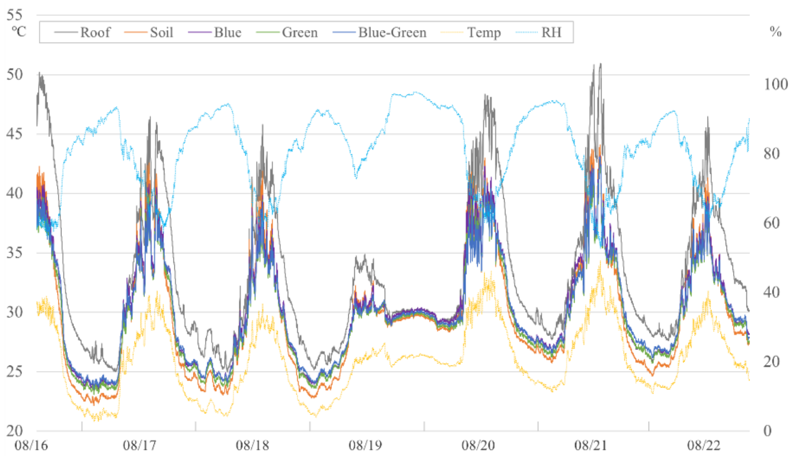

Fig. 29 Variations in upper surface temperature. Upper surface temperatures by roof type (Gray, Soil, Blue, Green, and Blue-Green) and meteorological data (air temperature and relative humidity) from 16/08/2022 to 22/08/2022.

Figure 29 shows the upper surface temperatures over a period of one week from August 16th to August 22nd. During this period, with the exception of the heavy rain on August 19th (66.1 mm/day), the environment was hot and humid, with daily maximum temperatures ranging from 30.3 ℃ to 34.3 ℃ and daily minimum relative humidity ranging from 52.7 % to 60.1 %. This allowed for the observation of the impact of the blue retention layer during clear weather conditions on the three days before and after the day with heavy rain.

The surface temperature of all roofs increased and decreased at a time similar to the air temperature; however, it was consistently higher than the air temperature at all times, especially during the day when the difference was greatly magnified owing to solar radiation. The experimental roofs always exhibited lower values than the gray roof, and that difference was greater during the day. Concrete has a low thermal conductivity compared to soil and water; therefore, it receives a relatively larger impact from solar radiation and air temperature.

2.2. Lower surface temperatures

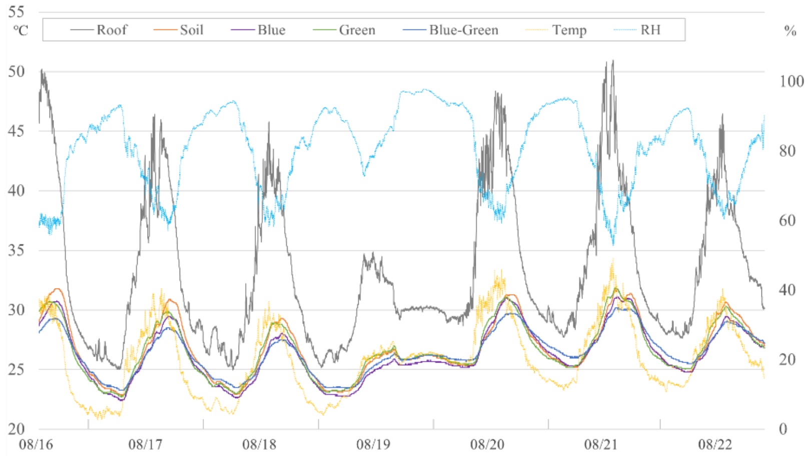

Fig. 30 Variation in the lower surface temperatures. Lower surface temperatures by roof type (Gray, Soil, Blue, Green, and Blue-Green) and meteorological data (air temperature and relative humidity) from 16/08/2022 to 22/08/2022.

The surface temperatures of the experimental roofs showed a much larger temperature decrease effect compared to that of the gray roof. As the sun's reflection is a major heat load in summer, the shadows caused by the modules had a significant impact. Blue-Green consistently had the lowest values, whereas Soil had the highest. The increase and decrease in the surface temperature of the experimental roofs showed a delayed pattern of 1–3 h compared to the ambient temperature, which was considered to be due to the time it took for heat to enter the upper layer and be conducted to the lower layer. Similar results have been reported in previous studies on heat lag (Kostadinović et al., 2022).

2.3. Performance evaluation

To quantitatively evaluate the thermal performance according to the roof type, surface temperatures were assessed using Welch's ANOVA and Games-Howell post-hoc tests for the entire measurement period because the homogeneity of variances was violated. The ANOVA test showed that, concerning the upper and lower surface temperatures, most of the time there was a low significant error rate ($p < 0.05$) and 95 % confidence level of significant difference between the average data of the Soil, Green, Blue, and Blue-Green roofs (Figure 30). The temperature-reduction effect based on the roof type exhibited various patterns in the upper and lower parts.

(a)

Time	Soil		Blue		Green		Blue-Green	
	P value	T value	P value	T value	P value	T value	P value	T value
00	***	2.38	***	1.34	***	1.65	***	1.29
01	***	2.31	***	1.35	***	1.63	***	1.30
02	***	2.01	***	1.04	***	1.43	***	1.08
03	***	1.90	***	0.84	***	1.33	***	0.95
04	***	1.74	***	0.67	***	1.13	***	0.75
05	***	1.60	*	0.56	***	0.97	**	0.61
06	***	1.28	ns	0.28	***	0.76	ns	0.36
07	*	0.75	ns	-0.42	ns	0.51	ns	-0.27
08	***	0.99	ns	-0.07	***	1.04	***	0.72
09	***	1.14	***	1.00	***	2.24	***	2.39
10	***	1.90	***	2.25	***	3.56	***	3.55
11	***	2.76	***	3.58	***	4.85	***	4.85
12	***	3.91	***	4.99	***	6.14	***	6.18
13	***	5.17	***	6.39	***	7.43	***	7.43
14	***	5.82	***	**6.67**	***	**7.59**	***	**7.54**
15	***	**6.13**	***	6.52	***	7.26	***	7.15
16	***	6.16	***	5.92	***	6.62	***	6.35
17	***	6.15	***	4.84	***	5.54	***	4.99
18	***	5.48	***	4.08	***	4.55	***	4.00
19	***	4.79	***	3.62	***	3.75	***	3.27
20	***	4.27	***	3.15	***	3.19	***	2.71
21	***	3.95	***	2.76	***	2.86	***	2.38
22	****	3.69	****	2.54	****	2.63	****	2.16
23	***	3.46	***	2.28	***	2.42	***	1.97

***p < .001, **p < .01, *p < .05, ns: not significance

(b)

Time	Soil		Blue		Green		Blue-Green	
	P value	T value	P value	T value	P value	T value	P value	T value
00	***	2.56	***	2.89	***	2.84	***	2.34
01	***	3.04	***	3.33	***	3.23	***	2.73
02	***	2.87	***	3.15	***	3.01	***	2.56
03	***	2.49	***	2.71	***	2.57	***	2.10
04	***	2.26	***	2.45	***	2.31	***	1.81
05	***	2.18	***	2.32	***	2.19	***	1.69
06	***	2.63	***	2.82	***	2.63	***	2.09
07	***	4.19	***	4.25	***	4.10	***	3.80
08	***	6.32	***	6.20	***	6.08	***	6.17
09	***	9.14	***	9.02	***	8.75	***	9.25
10	***	11.47	***	11.37	***	10.93	***	11.86
11	***	13.75	***	13.70	***	12.98	***	14.36
12	***	14.98	***	15.09	***	14.23	***	15.92
13	***	**16.02**	***	**16.36**	***	**15.55**	***	**17.35**
14	***	14.55	***	15.14	***	14.54	***	16.30
15	***	12.21	***	12.93	***	12.58	***	14.16
16	***	10.24	***	11.04	***	10.97	***	12.28
17	***	7.47	***	8.36	***	8.52	***	9.54
18	***	4.67	***	5.51	***	5.77	***	6.42
19	***	3.05	***	3.58	***	3.90	***	4.08
20	***	2.86	***	3.14	***	3.51	***	3.36
21	***	2.60	***	2.85	***	3.21	***	2.87
22	***	2.48	***	2.80	***	3.09	***	2.61
23	***	2.26	***	2.64	***	2.84	***	2.29

Fig. 31 Differences in surface temperatures. Mean differences and significance levels of the (a) upper and (b) lower surface temperatures between the gray roof and the other four experimental roof types over time.

The effect of reducing the daytime upper surface temperature was highest in the order of Green = Blue-Green > Blue > Soil, and albedo due to planting was considered to be the dominant factor. The measured albedo was 0.17 for the greenery and 0.12 for soil, and the planted modules showed an additional reduction of up to 2.2 ℃ over Soil and up to 1.3 ℃ over Blue (Figure A.2a). Despite having the same soil surface, it was found that Blue had a lower surface temperature owing to the high evaporation of acid. The upper surface temperatures of Green and Blue-Green were very similar, with no significant difference between them (Figure A.2a). At night, without solar radiation, the effect of reducing the upper surface temperature seemed to have played a major role in the order of temperature changes owing to specific heat and the amount of heat stored during the day. At night, when there was no solar radiation, temperatures changed in the order of Soil > Green > Blue > Blue-Green, and the variability in temperatures due to specific heat and the amount of heat stored during the day seemed to play a major role.

The effect of reducing daytime lower surface temperature was highest in the order of Blue-Green > Blue > Soil > Green, and it is believed that the blue retention layer was the dominant factor. The two roofs with blue retention layers (Blue-Green and Blue) were effective; Green, which did not have a blue retention layer, was the least effective until 13:00, after which Soil was the least effective. In particular, the Blue-Green had an additional reduction effect of up to 2.1 ℃ (Figure A.2b). Since the specific heat of water is five times that of dry soil, it was expected that the temperature increase would be small compared to the amount of heat introduced.

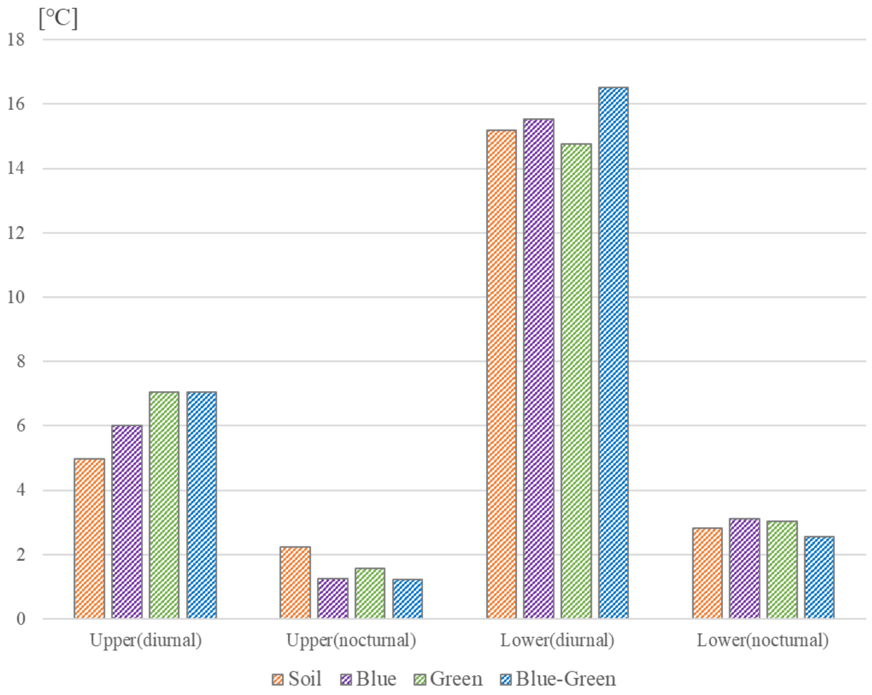

Fig. 32 Summary of thermal performance of roof type. Diurnal is from 1200 LST to 1400 LST, and nocturnal is from 0000 LST to 0200 LST.

Notably, Green was the least and Blue-Green the most effective, which can be interpreted as synergy between the planting and retention layers. Comparing the sum of the differences in Green~Soil and Blue~Soil and the values of Blue-Green~Soil, the synergy effect between Blue and Green was confirmed to be 1.49 ℃ on average from 11:00 to 14:00 (Figure A.3). Although there was no significant pattern during the night, the synergy effect between Green and Blue averaged -0.85 ℃ from 23:00 to 02:00, contrary to daytime results.

Owing to the experimental roof set-up, there was a difference of more than an hour between the upper and lower parts when the effect of temperature reduction was maximized. This result is consistent with those presented in Figure 32, which shows a delayed pattern compared with the increase or decrease in atmospheric temperature. The upper surface temperatures of the gray roof, soil, and vegetation increased with increasing solar radiation, but the lower surface temperature can be interpreted as the delayed conduction of incident heat resulting from shadows.

2.4. Heat balance

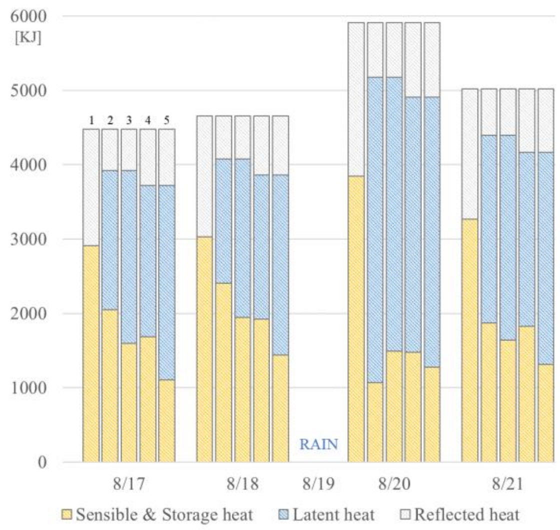

Fig. 33 Energy partition of solar radiation according to roof type. The daily total solar

radiation affecting the modules (0.25 m^2) and the energy balance of the reflected radiation measured using albedo and the latent heat from evapotranspiration ([1]Gray, [2]Soil, [3]Blue, [4]Green, and [5]Blue-Green) during the summer.

The latent heat flux calculated from the daily evapotranspiration through weight measurements and the reflected shortwaves calculated from the albedo allowed us to determine the amount of heat absorbed by the roof relative to the daily solar radiation (Figure 33). The albedo measurement showed that, with a value of 0.35, that of the Gray roof, was much larger than that of the Green (0.17) and Soil (0.12) ones, thus reflecting more solar radiation. However, it is believed that the temperature increased owing to the lack of latent heat and low specific heat compared to water and soil, particularly during the week.

On the day after the rain (8/20), the heat absorbed by the Soil roof was the lowest. Due to the heavy rainfall, all roof modules may have had sufficient water resources and, owing to the low layer of the Soil roof, a large amount of moisture may have remained in its upper layer. In addition, studies have reported that evapotranspiration is greater in the absence of plant cover under identical soil moisture conditions (Hodo-Abalo et al., 2012). Considering that rainfall occurred frequently during the measurement period, the thermal performance of the soil in this experiment would have been overestimated, and other modules may have a relatively greater temperature reduction effect in less rainy climates and regions.

Notably, although the Blue module reflected less solar radiation than the Green one owing to its low albedo, higher water availability induced more latent heat flux, resulting in similar absorbed heat; in fact, Blue and Green showed a competitive relationship at upper and lower surface temperatures (Figure A.2a and b). In general, the Blue-Green absorbed the least amount of heat owing to its high reflectance and high latent heat flux, as shown in Figure 32.

VI. Discussion & Conclusion

This study provides strategies to effectively mitigate the worsening urban heat environment worldwide. Firstly, a three-dimensional urban surface model (3D-USM) was proposed to comprehensively reflect complex urban spaces and evaluate the thermal environment using simple input data. Secondly, the model was validated by main parameters and result. And planting strategies for maximizing cooling effect of urban street trees and green wall were suggested by considering arrangement and area. Lastly, combination strategy of green roofs and blue retention layers was suggested by evaluation of the thermal performance and synergies in outdoor and indoor spaces. To achieve this, various types of roofs for the substrate (soil, retention, and greening layers) were quantitatively evaluated through experiments on thermal performance.

1. Developing a 3D urban surface model for accurate thermal evaluation with simple input

In the face of climate change and deteriorating UHIs, urban heat monitoring and evaluation are essential for achieving a sustainable society. The 3D-USM can be used as an evaluation tool when planning green areas in urban regions, as it can simulate the effects and changes when heat mitigation strategies are applied as well as diagnose the status quo. Furthermore, because the model is made of a flexible domain to simulate most structures, the model has the advantage of being applied to various cooling strategies, such as living walls and green roofs.

The 3D-USM model, which realistically reflects complex urban spaces, has limitations that should be improved upon in future studies. First, conduction is not considered for the heat transfer process. Using conduction, it would be possible to calculate the effect on the surrounding environment more accurately, and the heat value in the entire time zone would be reflected well in the next time zone (Meili et al., 2020; Z. H. Wang et al., 2011). Second, the artificial heat caused by buildings was not considered. As the buildings were not considered to be heat sources, they may have been overestimated as shadow providers (Taha, 1997). If artificial heat is reflected, buildings exposed to the sun produce increased artificial heat owing to high cooling energy demands, which can lead to an increase in surface temperature and deterioration of thermal comfort. Lastly, additional validation is necessary to confirm the applicability of the flexible model that can reflect various spaces, not only urban canyons. This would enhance the utility of the model.

Many studies have used the thermal comfort index received by humans for thermal environment analyses (Epstein & Moran, 2006; Salata et al., 2017). The MRT, an indicator developed to evaluate the heat received by humans, does not take into account the human thermoregulatory process and therefore cannot simulate human thermal comfort accurately. However, it is widely accepted that MRT plays an important role in the objective evaluation of thermal comfort (d'Ambrosio Alfano et al., 2021). MRT also serves as a key input for representative thermal comfort indices (PET, UTCI and PMV) and has been demonstrated to be effective in prior research (Krüger et al., 2011; Lai et al., 2017; Tan et al., 2013). The simulation MRT results using the proposed model have shown that detailed conditions of the surrounding environment can be reflected in the heat received by humans.

This model is composed of a grid of square shapes of a constant size in a 3D space, which allows for the potential to expand through coupling with various microclimate models. Through this, it is possible to expand from surface temperature to atmospheric temperature, or to expand to thermal comfort indices (PET, UTCI and PMV) from MRT.

Complementing these limitations and considering their applicability, the proposed 3D-USM, capable of accurately and efficiently simulating the thermal environment and MRT thermal comfort in complex urban environments using simple input data, holds great potential for guiding the development of efficient cooling strategies to foster sustainable cities.

2. Planting strategy for maximizing cooling effect of urban green infrastructure

When planning to install green infrastructure in your city, you need to achieve maximum cooling with limited space and budget. Street trees can provide pedestrians with direct cooling through shadows. Therefore, in order to maximize the cooling effect of trees, a strategy that considers shadows according to the direction of the street can be effective. Overall, our simulation results that the northern street showing a worse thermal environment than the southern street are consistent with the results of previous studies (Ali-Toudert & Mayer, 2006; Taleghani et al., 2015). MRT was reduced by 15-18 ℃ due to the shading effect of buildings, which is consistent with a study conducted in Singapore, which has a similar climate (Mirzaei et al., 2015).

This study further focused on the angular changes in the E–W street and found that the thermal environment changes even with small changes in the street direction. The MRT of the northern sidewalk of the street rotated by 12.5° was 2.6 ℃ lower on an average than that of sidewalk of the street that was not rotated (53.6 ℃ and 56.2 ℃ in Streets 1 and 2, respectively). Even under the same conditions under which direct radiation is received, surrounding urban elements, including nearby south-facing buildings, emit high longwave radiant heat owing to receiving a large amount of heat, consequently increasing the MRT level. Depending on the orientation of the street, the location where cooling was required changed with time, and this was further confirmed via a street tree-planting simulation. The results imply that even small variations in the angle of the street can significantly impact thermal comfort over time, resulting in different optimal locations for effective vegetation. Therefore, streets in the same E–W direction need appropriate strategies depending on the its angle.

In the case of green wall, the cooling effect provided to pedestrians has changed significantly depending on the placement height. As the height increased, it provided less cooling effect to pedestrians, and this study proved that there is a cost-effective height and area through analysis of MRT reduction effect by area. Although green wall provides a relatively small cooling effect compared to street trees that provide shadows, it can be an efficient cooling strategy for urban spaces where street trees are difficult to deploy. This result suggests that spatiotemporal thermal comfort simulations considering the angle of the streets and simulation based planning are necessary for efficiently cooling cities. The flexible 3D-USM developed to reflect a range of urban spaces and strategies, including gray and green infrastructure, is expected to become a useful tool in planning for thermally comfortable urban spaces.

3. Blue green roof strategy for improving thermal performance in outdoor and indoor spaces

Reducing the roof surface temperature through the greening of buildings results in indoor cooling energy savings (Berardi, 2016; Refahi & Talkhabi, 2015; Silva et al., 2016; Virk et al., 2015). Akbari (2002) simulated building energy consumption from green roof in California and confirmed a 30 % energy saving and a significant CO2 emission reduction effect. The experimental results of the present study showed that the surface temperature can be reduced by 15.50 ℃ between 12:00 and 14:00 by covering shadows with soil, thereby greatly reducing the amount of heat flowing into the building. The temperature reduction of the Blue roof was 15.73 ℃, which did not differ much from Soil, and that of Green and Blue-Green was 14.89 ℃ and 16.64 ℃, respectively, representing the minimum and maximum. It is possible that the Soil module effect was overestimated because large amounts of rainfall occurred during the measurement period.

Cai et al. (2019) evaluated the thermal insulation performance of a green roof through indoor and outdoor surface temperature measurements, showing that the green roof reduced the outdoor surface temperature by 15 ℃ and caused a 5 ℃ difference in indoor surface temperature. Considering that this result is similar to the reduction in the lower surface temperature measured in this study, the energy-saving effect of the experimental roof could have been sufficiently significant, and an even larger effect could be expected when applying a Blue-Green roof.

Urban greening is a representative strategy for improving hot environments and mitigating UHI effects (Aram et al., 2019; Roth et al., 1989; Wong et al., 2021). Trees significantly improve hot environments owing to shading of the pedestrian areas and the transpiration effect (B. S. Lin & Lin, 2010). A study conducted in Toronto also reported a 0.4 ℃ air temperature cooling at the pedestrian level (Berardi, 2016). Lin et al. (2021) found that green roofs play an important role in regulating the thermal environment in areas without large green or water spaces. In the experiment conducted in this study, green spaces played an important role in the upper surface temperature, which affected the outdoor thermal environment (Figure 16a). Considering the costs, a green roof without a blue retention layer would be a good strategy for improving the thermal environment in low-rise areas.

Analyzing the synergies of Green and Blue by comparing the effects of individual and simultaneous application highlighted different patterns in the upper and lower surface temperatures and between day and night (Figure A.3). During the daytime (12:00–14:00), the synergy effect was +1.12 ℃ in the upper and an -1.59 ℃ in the lower surface temperature, and during the night, the opposite was observed (upper and lower surface temperatures of -0.65 ℃ and +0.80 ℃, respectively). Considering the period during which the thermal environment is at its worst, the blue retention layer may be ineffective during the daytime if the goal is to improve outdoor thermal comfort.

However, if the goal is to improve indoor thermal comfort and reduce energy consumption, a Blue-Green roof may be an efficient strategy for generating additional synergies. (Rozos et al., 2013) reported that when both green and blue technologies are installed simultaneously, the drawbacks of each can be minimized and the benefits combined, which is consistent with our conclusion that the Blue-Green roof was the most effective for reducing both the upper and lower surface temperatures during the daytime. Additionally, our results showed that the effect of the Blue-Green roof was magnified in hot and dry climates and regions (Figure A.4).

This study provides strategies to effectively mitigate the worsening urban heat environment worldwide. A three-dimensional urban surface model was developed to diagnose heat status by quickly simulating complex urban spaces with simple input data, identifying vulnerable areas and evaluating the effects of various cooling strategies and scenarios.

As a representative green infrastructure, we focused on tree planting, green walls, and green roof, providing strategies to enhance the cooling effect of green infrastructure. Trees offer the most significant cooling effect for pedestrians by providing shade, and their effective placement is essential considering the varying shadow conditions depending on the orientation of streets and buildings. Green walls, on the other hand, require appropriate height selection to ensure cost-effective cooling effects, as the cooling effect diminishes significantly with increasing height. Lastly, green roof was proposed as a strategy to effectively improve outdoor and indoor thermal environments by combining it with a blue retention layer to increase latent heat transfer. Quantitative experiments were conducted to confirm the effectiveness of this approach.

This study has the potential to inform urban planners and decision-makers about the most effective strategies for promoting sustainable cities and help shape the future of urban environments in a more sustainable direction.

VII. Bibliography

Achour-Younsi, Safa, and Fakher Kharrat. 2016. "Outdoor Thermal Comfort: Impact of the Geometry of an Urban Street Canyon in a Mediterranean Subtropical Climate – Case Study Tunis, Tunisia." Procedia - Social and Behavioral Sciences 216(October 2015):689–700.

Afshari, Afshin, and Nicolas Ramirez. 2021. "Improving the Accuracy of Simplified Urban Canopy Models for Arid Regions Using Site-Specific Prior Information." Urban Climate 35(November 2020):100722.

Akbari, H. 2002. "Shade Trees Reduce Building Energy Use and CO2 Emissions from Power Plants." Environmental Pollution 116(SUPPL. 1):119–26.

Ali-Toudert, Fazia, and Helmut Mayer. 2006. "Numerical Study on the Effects of Aspect Ratio and Orientation of an Urban Street Canyon on Outdoor Thermal Comfort in Hot and Dry Climate." Building and Environment 41(2):94–108.

Allam, Zaheer, and David S. Jones. 2021. "Future (Post-COVID) Digital, Smart and Sustainable Cities in the Wake of 6G: Digital Twins, Immersive Realities and New Urban Economies." Land Use Policy 101(December 2020):105201.

Allen, R. G., L. S. Pereira, D. Raes, and M. Smith. 1998. "Crop Evapotranspiration-Guidelines for Computing Crop Water Requirements-FAO Irrigation and Drainage Paper 56." Fao 300(9).

Andenæs, Erlend, Tore Kvande, Tone M. Muthanna, and Jardar Lohne. 2018. "Performance of Blue-Green Roofs in Cold Climates: A Scoping Review." Buildings 8(4).

Aram, Farshid, Ester Higueras García, Ebrahim Solgi, and Soran Mansournia. 2019. "Urban Green Space Cooling Effect in Cities." Heliyon 5(4):e01339.

Armson, D., P. Stringer, and A. R. Ennos. 2012. "The Effect of Tree Shade and Grass on Surface and Globe Temperatures in an Urban Area." Urban Forestry & Urban Greening 11(3):245–55.

Åström, Daniel Oudin, Bertil Forsberg, and Joacim Rocklöv. 2011. "Heat Wave Impact on Morbidity and Mortality in the Elderly Population: A Review of

Recent Studies." Maturitas 69(2):99–105.

Bai, Xuemei, Indira Nath, Anthony Capon, Nordin Hasan, and Dov Jaron. 2012. "Health and Wellbeing in the Changing Urban Environment: Complex Challenges, Scientific Responses, and the Way Forward." Current Opinion in Environmental Sustainability 4(4):465–72.

Baldocchi, Dennis, and Tilden Meyers. 1998. "On Using Eco-Physiological, Micrometeorological and Biogeochemical Theory to Evaluate Carbon Dioxide, Water Vapor and Trace Gas Fluxes over Vegetation: A Perspective." Agricultural and Forest Meteorology 90(1–2):1–25.

Ball, J. Timothy, Ian E. Woodrow, and Joseph A. Berry. 1987. "A Model Predicting Stomatal Conductance and Its Contribution to the Control of Photosynthesis under Different Environmental Conditions BT - Progress in Photosynthesis Research: Volume 4 Proceedings of the VIIth International Congress on Photosynthesis Pr." Pp. 221–24 in, edited by J. Biggins. Dordrecht: Springer Netherlands.

Benvenuti, Stefano, and Davide Bacci. 2010. "Initial Agronomic Performances of Mediterranean Xerophytes in Simulated Dry Green Roofs." Urban Ecosystems 13(3):349–63.

Berardi, Umberto. 2016. "The Outdoor Microclimate Benefits and Energy Saving Resulting from Green Roofs Retrofits." Energy and Buildings 121:217–29.

Berndtsson, Justyna Czemiel, Lars Bengtsson, and Kenji Jinno. 2009. "Runoff Water Quality from Intensive and Extensive Vegetated Roofs." Ecological Engineering 35(3):369–80.

Bhagavathula, Susila, Katja Brundiers, Michael Stauffacher, and Braden Kay. 2021. "Fostering Collaboration in City Governments' Sustainability, Emergency Management and Resilience Work through Competency-Based Capacity Building." International Journal of Disaster Risk Reduction 63:102408.

Block, Annie Hunter, Stephen J. Livesley, and Nicholas S. G. Williams. 2012. "Responding to the Urban Heat Island : A Review of the Potential of Green

Infrastructure." Victorian Centre for Climate Change Adaptation 1–62.

Blocken, Bert. 2015. "Computational Fluid Dynamics for Urban Physics: Importance, Scales, Possibilities, Limitations and Ten Tips and Tricks towards Accurate and Reliable Simulations." Building and Environment 91:219–45.

Bruse, Michael, and Heribert Fleer. 1998. "Simulating Surface-Plant-Air Interactions inside Urban Environments with a Three Dimensional Numerical Model." Environmental Modelling and Software 13(3–4):373–84.

Buck, A. L. 1981. "New Equations for Computing Vapour Pressure and Enhancement Factor." Journal of Applied Meteorology 20(12):1527–32.

Buck, A. L. 2012. "Humidity Conversion Equations." Model CR-1A Hygrometer with Autofill, Operating Manual (1930):20–21.

Busker, Tim, Hans de Moel, Toon Haer, Maurice Schmeits, Bart van den Hurk, Kira Myers, Dirk Gijsbert Cirkel, and Jeroen Aerts. 2022. "Blue-Green Roofs with Forecast-Based Operation to Reduce the Impact of Weather Extremes." Journal of Environmental Management 301(June 2021):113750.

Cai, Lu, Xiao Ping Feng, Jing Yan Yu, Qian Chao Xiang, and Rui Chen. 2019. "Reduction in Carbon Dioxide Emission and Energy Savings Obtained by Using a Green Roof." Aerosol and Air Quality Research 19(11):2432–45.

Campbell, Gaylon S., and John M. Norman. 1998. An Introduction to Environmental Biophysics. New York, NY: Springer New York.

Cascone, Stefano, Antonio Gagliano, Tiziana Poli, and Gaetano Sciuto. 2019. "Thermal Performance Assessment of Extensive Green Roofs Investigating Realistic Vegetation-Substrate Configurations." Building Simulation 12(3):379–93.

Charalambous, Katerina, Adriana Bruggeman, Marinos Eliades, Corrado Camera, and Loukia Vassiliou. 2019. "Stormwater Retention and Reuse at the Residential Plot Level—Green Roof Experiment and Water Balance Computations for Long-Term Use in Cyprus." Water 11(5):1055.

Chen, Fei, Hiroyuki Kusaka, Robert Bornstein, Jason Ching, C. S. B. Grimmond, Susanne Grossman-Clarke, Thomas Loridan, Kevin W. Manning, Alberto

Martilli, Shiguang Miao, David Sailor, Francisco P. Salamanca, Haider Taha, Mukul Tewari, Xuemei Wang, Andrzej A. Wyszogrodzki, and Chaolin Zhang. 2011. “The Integrated WRF/Urban Modelling System: Development, Evaluation, and Applications to Urban Environmental Problems.” International Journal of Climatology 31(2):273–88.

Choudhury, B. J., and J. L. Monteith. 1988. “A Four-layer Model for the Heat Budget of Homogeneous Land Surfaces.” Quarterly Journal of the Royal Meteorological Society 114(480):373–98.

Collatz, G. James, J. Timothy Ball, Cyril Grivet, and Joseph A. Berry. 1991. “Physiological and Environmental Regulation of Stomatal Conductance, Photosynthesis and Transpiration: A Model That Includes a Laminar Boundary Layer.” Agricultural and Forest Meteorology 54(2–4):107–36.

Cristiano, Elena, Antonio Annis, Ciro Apollonio, Dario Pumo, Salvatore Urru, Francesco Viola, Roberto Deidda, Raffaele Pelorosso, Andrea Petroselli, Flavia Tauro, Salvatore Grimaldi, Antonio Francipane, Francesco Alongi, Leonardo Valerio Noto, Olivier Hoes, Friso Klapwijk, Brian Schmitt, and Fernando Nardi. 2022. “Multilayer Blue-Green Roofs as Nature-Based Solutions for Water and Thermal Insulation Management.” Hydrology Research 53(9):1129–49.

Cristiano, Elena, Roberto Deidda, and Francesco Viola. 2021. “The Role of Green Roofs in Urban Water-Energy-Food-Ecosystem Nexus: A Review.” Science of the Total Environment 756:143876.

d’Ambrosio Alfano, Francesca Romana, Marco Dell’isola, Giorgio Ficco, Boris Igor Palella, and Giuseppe Riccio. 2021. “On the Measurement of the Mean Radiant Temperature by Means of Globes: An Experimental Investigation under Black Enclosure Conditions.” Building and Environment 193(February):107655.

Dai, Yongjiu, Robert E. Dickinson, and Ying-Ping Wang. 2004. “A Two-Big-Leaf Model for Canopy Temperature, Photosynthesis, and Stomatal Conductance.” Journal of Climate 17(12):2281–99.

Doick, Kieron, and Tony Hutchings. 2013. “Air Temperature Regulation by Urban Trees and Green Infrastructure.” Forestry Commission, Research Note (February):1–10.

Dong, Jing, Meixia Lin, Jin Zuo, Tao Lin, Jiakun Liu, Caige Sun, and Jiancheng Luo. 2020. “Quantitative Study on the Cooling Effect of Green Roofs in a High-Density Urban Area—A Case Study of Xiamen, China.” Journal of Cleaner Production 255:120152.

Du, Jing, Cheng Sun, Qiuke Xiao, Xin Chen, and Jing Liu. 2020. “Field Assessment of Winter Outdoor 3-D Radiant Environment and Its Impact on Thermal Comfort in a Severely Cold Region.” Science of the Total Environment 709(66):136175.

Ehlert, J. R., and T. F. Smith. 1993. “View Factors for Perpendicular and Parallel Rectangular Plates.” Journal of Thermophysics and Heat Transfer 7(1):173–75.

Epstein, Yoram, and Daniel S. Moran. 2006. “Thermal Comfort and the Heat Stress Indices.” Industrial Health 44(3):388–98.

Erbs, D. G., S. A. Klein, and J. A. Duffie. 1982. “Estimation of the Diffuse Radiation Fraction for Hourly, Daily and Monthly-Average Global Radiation.” Solar Energy 28(4):293–302.

Ercolani, Giulia, Enrico Antonio Chiaradia, Claudio Gandolfi, Fabio Castelli, and Daniele Masseroni. 2018. “Evaluating Performances of Green Roofs for Stormwater Runoff Mitigation in a High Flood Risk Urban Catchment.” Journal of Hydrology 566(September):830–45.

Evans, John R. 1989. “Photosynthesis and Nitrogen Relationships in Leaves of C3 Plants.” Oecologia 78(1):9–19.

Fabbri, K., and V. Costanzo. 2020. “Drone-Assisted Infrared Thermography for Calibration of Outdoor Microclimate Simulation Models.” Sustainable Cities and Society 52(September 2019):101855.

Fantozzi, Fabio, Carlo Bibbiani, Caterina Gargari, Roberto Rugani, and Giacomo Salvadori. 2021. “Do Green Roofs Really Provide Significant Energy Saving in a Mediterranean Climate? Critical Evaluation Based on Different Case Studies.” Frontiers of Architectural Research 10(2):447–65.

Farquhar, G. D., S. von Caemmerer, and J. A. Berry. 1980. “A Biochemical Model of Photosynthetic CO2 Assimilation in Leaves of C3 Species.” Planta 149(1):78–90.

Fatichi, Simone. 2010. “The Modeling of Hydrological Cycle and Its Interaction with Vegetation in the Framework of Climate Change.” University of Firenze (March 2010):463.

Field, C. 1983. “Allocating Leaf Nitrogen for the Maximization of Carbon Gain: Leaf Age as a Control on the Allocation Program.” Oecologia 56(2–3):341–47.

Gagliano, A., M. Detommaso, F. Nocera, F. Patania, and S. Aneli. 2014. “The Retrofit of Existing Buildings through the Exploitation of the Green Roofs - A Simulation Study.” Energy Procedia 62:52–61.

Gál, Csilla V., and Noémi Kántor. 2020. “Modeling Mean Radiant Temperature in Outdoor Spaces, A Comparative Numerical Simulation and Validation Study.” Urban Climate 32(November 2019):100571.

Getter, Kristin L., D. Bradley Rowe, G. Philip Robertson, Bert M. Cregg, and Jeffrey A. Andresen. 2009. “Carbon Sequestration Potential of Extensive Green Roofs.” Environmental Science & Technology 43(19):7564–70.

González, Jorge E., Prathap Ramamurthy, Robert D. Bornstein, Fei Chen, Elie R. Bou-Zeid, Masoud Ghandehari, Jeffrey Luvall, Chandana Mitra, and Dev Niyogi. 2021. “Urban Climate and Resiliency: A Synthesis Report of State of the Art and Future Research Directions.” Urban Climate 38(April).

Grimmond, C. S. B., and T. R. Oke. 1999. “Heat Storage in Urban Areas: Local-Scale Observations and Evaluation of a Simple Model.” Journal of Applied Meteorology 38(7):922–40.

Grimmond, C. S. B., H. A. Cleugh, and T. R. Oke. 1991. “An Objective Urban Heat Storage Model and Its Comparison with Other Schemes.” Atmospheric Environment. Part B. Urban Atmosphere 25(3):311–26.

Guan, Dexin, Ting-yao Zhu, and Shi-jie Han. 2000. "Wind Tunnel Experiment of Drag of Isolated Tree Models in Surface Boundary Layer." Journal of Forestry Research 11(3):156–60.

Guan, Dexin, Yushu Zhang, and Tingyao Zhu. 2003. "A Wind-Tunnel Study of Windbreak Drag." Agricultural and Forest Meteorology 118(1–2):75–84.

Harley, P. C., and J. D. Tenhunen. 1991. "Modeling the Photosynthetic Response of C3 Leaves to Environmental Factors." Modeling Crop Photosynthesis—from Biochemistry to Canopy 17–39.

Harley, P. C., R. B. Thomas, J. F. Reynolds, and B. R. Strain. 1992. "Modelling Photosynthesis of Cotton Grown in Elevated CO2." Plant, Cell & Environment 15(3):271–82.

Harmay, Nurul Syahira Mohammad, and Minha Choi. 2023. "The Urban Heat Island and Thermal Heat Stress Correlate with Climate Dynamics and Energy Budget Variations in Multiple Urban Environments." Sustainable Cities and Society 91(July 2022):104422.

He, Bao Jie, Lan Ding, and Deo Prasad. 2020b. "Urban Ventilation and Its Potential for Local Warming Mitigation: A Field Experiment in an Open Low-Rise Gridiron Precinct." Sustainable Cities and Society 55(January):102028.

Hetherington, A. M., and F. l. Woodward. 2003. "The Role of Stomata in Sensing and Driving Environmental Change." Nature 424(August):528–39.

Hodo-Abalo, Samah, Magolmèèna Banna, and Belkacem Zeghmati. 2012. "Performance Analysis of a Planted Roof as a Passive Cooling Technique in Hot-Humid Tropics." Renewable Energy 39(1):140–48.

Höppe, P. 1999. "The Physiological Equivalent Temperature - a Universal Index for the Biometeorological Assessment of the Thermal Environment." International Journal of Biometeorology 43(2):71–75.

Howell, John R., M. Pinar Menguc, and Robert Siegel. 2010. Thermal Radiation Heat Transfer. CRC Press.

Imran, H. M., J. Kala, A. W. M. Ng, and S. Muthukumaran. 2018. "Effectiveness of Green and Cool Roofs in Mitigating Urban Heat Island Effects during a

Heatwave Event in the City of Melbourne in Southeast Australia." Journal of Cleaner Production 197:393–405.

Intergovernmental Panel on Climate Change. 2014. Climate Change 2013 – The Physical Science Basis: Working Group I Contribution to the Fifth Assessment Report of the Intergovernmental Panel on Climate Change. Cambridge: Cambridge University Press.

IPCC. 2007. Climate Change 2007 - Fourth Assessment Report. Intergovernmental Panel on Climate Change.

Jänicke, Britta, Dragan Milošević, and Suneja Manavvi. 2021. "Review of User-friendly Models to Improve the Urban Micro-climate." Atmosphere 12(10):1–22.

Jim, C. Y., and S. W. Tsang. 2011. "Ecological Energetics of Tropical Intensive Green Roof." Energy and Buildings 43(10):2696–2704.

Johnson, I. R., and J. H. M. Thornley. 1985. "Temperature Dependence of Plant and Crop Process." Annals of Botany 55(1):1–24.

Jones, Hamlyn. 1983. "Plants and Microclimate."

Jordan, Douglas B., and William L. Ogren. 1984. "The CO 2 /O 2 Specificity of Ribulose 1,5-Bisphosphate Carboxylase/Oxygenase - Dependence on Ribulosebisphosphate Concentration, PH and Temperature." Planta 161(4):308–13.

Kanda, M., T. Kawai, M. Kanega, R. Moriwaki, K. Narita, and A. Hagishima. 2005. "A Simple Energy Balance Model for Regular Building Arrays." Boundary-Layer Meteorology 116(3):423–43.

Karimimoshaver, Mehrdad, Rezvan Khalvandi, and Mohammad Khalvandi. 2021. "The Effect of Urban Morphology on Heat Accumulation in Urban Street Canyons and Mitigation Approach." Sustainable Cities and Society 73(March):103127.

Kent, Christoph W., Sue Grimmond, and David Gatey. 2017. "Aerodynamic Roughness Parameters in Cities: Inclusion of Vegetation." Journal of Wind Engineering and Industrial Aerodynamics 169(July):168–76.

Konarska, Janina, Johan Uddling, Björn Holmer, Martina Lutz, Fredrik Lindberg, Håkan Pleijel, and Sofia Thorsson. 2016. "Transpiration of Urban Trees and Its Cooling Effect in a High Latitude City." International Journal of Biometeorology 60(1):159–72.

Kostadinović, Danka, Marina Jovanović, Vukman Bakić, Nenad Stepanić, and Maja Todorović. 2022. "Experimental Investigation of Summer Thermal Performance of the Green Roof System with Mineral Wool Substrate." Building and Environment 217:109061.

Krüger, E. L., F. O. Minella, and F. Rasia. 2011. "Impact of Urban Geometry on Outdoor Thermal Comfort and Air Quality from Field Measurements in Curitiba, Brazil." Building and Environment 46(3):621–34.

La Roche, Pablo, and Umberto Berardi. 2014. "Comfort and Energy Savings with Active Green Roofs." Energy and Buildings 82:492–504.

Lai, Alan, Minjung Maing, and Edward Ng. 2017. "Observational Studies of Mean Radiant Temperature across Different Outdoor Spaces under Shaded Conditions in Densely Built Environment." Building and Environment 114:397–409.

Le Roux, X., H. Sinoquet, and M. Vandame. 1999. "Spatial Distribution of Leaf Dry Weight per Area and Leaf Nitrogen Concentration in Relation to Local Radiation Regime within an Isolated Tree Crown." Tree Physiology 19(3):181–88.

Le Roux, X., S. Grand, E. Dreyer, and F. A. Daudet. 1999. "Parameterization and Testing of a Biochemically Based Photosynthesis Model for Walnut (Juglans Regia) Trees and Seedlings." Tree Physiology 19(8):481–92.

Lee, Hyunjung, and Helmut Mayer. 2016. "Validation of the Mean Radiant Temperature Simulated by the RayMan Software in Urban Environments." International Journal of Biometeorology 60(11):1775–85.

Leuning, R., Y. P. Wang, and R. N. Cromer. 1991. "Model Simulations of Spatial Distributions and Daily Totals of Photosynthesis in Eucalyptus Grandis Canopies." Oecologia 88(4):494–503.

Li, Hong, and Tai-Ho Kang. 2013. “Photosynthetic Characteristics of Sedum Takevimense on Various Moisture Conditions in a Green Roof System.” Journal of the Korean Institute of Landscape Architecture 41(6):140–46.

Li, Shu-xiao, Hua-peng Qin, Yue-nuan Peng, and Soon Thiam Khu. 2019. “Modelling the Combined Effects of Runoff Reduction and Increase in Evapotranspiration for Green Roofs with a Storage Layer.” Ecological Engineering 127(July 2018):302–11.

Li, Yunfei, Sebastian Schubert, Jürgen P. Kropp, and Diego Rybski. 2020. “On the Influence of Density and Morphology on the Urban Heat Island Intensity.” Nature Communications 11(1):1–9.

Lin, Bau Show, and Yann Jou Lin. 2010. “Cooling Effect of Shade Trees with Different Characteristics in a Subtropical Urban Park.” HortScience 45(1):83–86.

Lin, Borong, Xiaofeng Li, Yingxin Zhu, and Youguo Qin. 2008. “Numerical Simulation Studies of the Different Vegetation Patterns’ Effects on Outdoor Pedestrian Thermal Comfort.” Journal of Wind Engineering and Industrial Aerodynamics 96(10–11):1707–18.

Lin, Meixia, Jing Dong, Laurence Jones, Jiakun Liu, Tao Lin, Jin Zuo, Hong Ye, Guoqin Zhang, and Tiejun Zhou. 2021. “Modeling Green Roofs’ Cooling Effect in High-Density Urban Areas Based on Law of Diminishing Marginal Utility of the Cooling Efficiency: A Case Study of Xiamen Island, China.” Journal of Cleaner Production 316(July).

Lindberg, Fredrik, and C. S. B. Grimmond. 2011. “Nature of Vegetation and Building Morphology Characteristics across a City: Influence on Shadow Patterns and Mean Radiant Temperatures in London.” Urban Ecosystems 14(4):617–34.

Lindberg, Fredrik, Björn Holmer, and Sofia Thorsson. 2008. “SOLWEIG 1.0 - Modelling Spatial Variations of 3D Radiant Fluxes and Mean Radiant Temperature in Complex Urban Settings.” International Journal of Biometeorology 52(7):697–713.

Liu, Haimeng, Weijia Cui, and Mi Zhang. 2022. “Exploring the Causal Relationship between Urbanization and Air Pollution: Evidence from China.” Sustainable Cities and Society 80(January):103783.

Loescher, H. W., C. V. Hanson, and T. W. Ocheltree. 2009. “The Psychrometric Constant Is Not Constant: A Novel Approach to Enhance the Accuracy and Precision of Latent Energy Fluxes through Automated Water Vapor Calibrations.” Journal of Hydrometeorology 10(5):1271–84.

Lumley, Thomas, Paula Diehr, Scott Emerson, and Lu Chen. 2002. “The Importance of the Normality Assumption in Large Public Health Data Sets.” Annual Review of Public Health 23(1):151–69.

Luo, Kun, Xuebin Hu, Qiang He, Zhengsong Wu, Hao Cheng, Zhenlong Hu, and Asit Mazumder. 2018. “Impacts of Rapid Urbanization on the Water Quality and Macroinvertebrate Communities of Streams: A Case Study in Liangjiang New Area, China.” Science of the Total Environment 621:1601–14.

Macdonald, R. W., R. F. Griffiths, and D. J. Hall. 1998. “An Improved Method for the Estimation of Surface Roughness of Obstacle Arrays.” Atmospheric Environment 32(11):1857–64.

Mahat, Vinod, David G. Tarboton, and Noah P. Molotch. 2013. “Testing Above- and below-Canopy Representations of Turbulent Fluxes in an Energy Balance Snowmelt Model.” Water Resources Research 49(2):1107–22.

Manoli, Gabriele, Simone Fatichi, Markus Schläpfer, Kailiang Yu, Thomas W. Crowther, Naika Meili, Paolo Burlando, Gabriel G. Katul, and Elie Bou-Zeid. 2019. “Magnitude of Urban Heat Islands Largely Explained by Climate and Population.” Nature 573(7772):55–60.

Masson, Valéry. 2000. “A Physically-Based Scheme for the Urban Energy Budget in Atmospheric Models.” Boundary-Layer Meteorology 94(3):357–97.

Matzarakis, Andreas, Frank Rutz, and Helmut Mayer. 2007. “Modelling Radiation Fluxes in Simple and Complex Environments - Application of the RayMan Model.” International Journal of Biometeorology 51(4):323–34.

McPhearson, Timon, Dagmar Haase, Nadja Kabisch, and Åsa Gren. 2016.

“Advancing Understanding of the Complex Nature of Urban Systems.” Ecological Indicators 70:566–73.

McPhearson, Timon, Erik Andersson, Thomas Elmqvist, and Niki Frantzeskaki. 2015. “Resilience of and through Urban Ecosystem Services.” Ecosystem Services 12:152–56.

Meili, Naika, Gabriele Manoli, Paolo Burlando, Elie Bou-Zeid, Winston T. L. Chow, Andrew M. Coutts, Edoardo Daly, Kerry A. Nice, Matthias Roth, Nigel J. Tapper, Erik Velasco, Enrique R. Vivoni, and Simone Fatichi. 2020. “An Urban Ecohydrological Model to Quantify the Effect of Vegetation on Urban Climate and Hydrology (UT&C v1.0).” Geoscientific Model Development 13(1):335–62.

Middel, Ariane, Kathrin Häb, Anthony J. Brazel, Chris A. Martin, and Subhrajit Guhathakurta. 2014. “Impact of Urban Form and Design on Mid-Afternoon Microclimate in Phoenix Local Climate Zones.” Landscape and Urban Planning 122:16–28.

Mirzaei, Parham A. 2021. “CFD Modeling of Micro and Urban Climates: Problems to Be Solved in the New Decade.” Sustainable Cities and Society 69(March):102839.

Mirzaei, Parham A., and Fariborz Haghighat. 2010. “Approaches to Study Urban Heat Island - Abilities and Limitations.” Building and Environment 45(10):2192–2201.

Mirzaei, Parham A., Dave Olsthoorn, Michael Torjan, and Fariborz Haghighat. 2015. “Urban Neighborhood Characteristics Influence on a Building Indoor Environment.” Sustainable Cities and Society 19(8):403–13.

Narayana, K. Badari. 1998. “View Factors for Parallel Rectangular Plates.” Heat Transfer Engineering 19(1):59–63.

Nguyen, Cuong Ngoc, Nitin Muttil, Muhammad Atiq Ur Rehman Tariq, and Anne W. M. Ng. 2022. “Quantifying the Benefits and Ecosystem Services Provided by Green Roofs—A Review.” Water (Switzerland) 14(1).

Niachou, A., K. Papakonstantinou, M. Santamouris, A. Tsangrassoulis, and G.

Mihalakakou. 2001. “Analysis of the Green Roof Thermal Properties and Investigation of Its Energy Performance.” Energy and Buildings 33(7):719–29.

Nice, Kerry A., Andrew M. Coutts, and Nigel J. Tapper. 2018. “Development of the VTUF-3D v1.0 Urban Micro-Climate Model to Support Assessment of Urban Vegetation Influences on Human Thermal Comfort.” Urban Climate 24(November 2017):1052–76.

Nunez, M., and T. R. Oke. 1977. “The Energy Balance of an Urban Canyon.” Journal of Applied Meteorology 16(1):11–19.

Oberndorfer, Erica, Jeremy Lundholm, Brad Bass, Reid R. Coffman, Hitesh Doshi, Nigel Dunnett, Stuart Gaffin, Manfred Köhler, Karen K. Y. Liu, and Bradley Rowe. 2007. “Green Roofs as Urban Ecosystems: Ecological Structures, Functions, and Services.” BioScience 57(10):823–33.

Oke, T. R. 1973. “City Size and the Urban Heat Island.” Atmospheric Environment (1967) 7(8):769–79.

Oke, T. R. 1982. “The Energetic Basis of the Urban Heat Island.” Quarterly Journal of the Royal Meteorological Society 108(455):1–24.

Okeil, Ahmad. 2010. “A Holistic Approach to Energy Efficient Building Forms.” Energy and Buildings 42(9):1437–44.

Park, Chae Yeon, Dong Kun Lee, E. Scott Krayenhoff, Han Kyul Heo, Saekyul Ahn, Takashi Asawa, Akinobu Murakami, and Ho Gul Kim. 2018. “A Multilayer Mean Radiant Temperature Model for Pedestrians in a Street Canyon with Trees.” Building and Environment 141(March):298–309.

Park, Chae Yeon, Dong Kun Lee, E. Scott Krayenhoff, Han Kyul Heo, Saekyul Ahn, Takashi Asawa, Akinobu Murakami, and Ho Gul Kim. 2018. “A Multilayer Mean Radiant Temperature Model for Pedestrians in a Street Canyon with Trees.” Building and Environment 141(March):298–309.

Peng, Lilliana L. H., and C. Y. Jim. 2013. “Green-Roof Effects on Neighborhood Microclimate and Human Thermal Sensation.” Energies 6(2):598–618.

Pimentel-Rodrigues, C., and A. Silva-Afonso. 2018. “Adaptation Measures to

Climate Change . Integration of Green Roofs with Rainwater Harvesting Systems 2 Run-off Coefficients in Conventional." WSEAS Transactions on Environment and Development 14:53–61.

Prentice, I. Colin, Ning Dong, Sean M. Gleason, Vincent Maire, and Ian J. Wright. 2014. "Balancing the Costs of Carbon Gain and Water Transport: Testing a New Theoretical Framework for Plant Functional Ecology." Ecology Letters 17(1):82–91.

Pumo, Dario, Antonio Francipane, Francesco Alongi, and Leonardo V. Noto. 2023. "The Potential of Multilayer Green Roofs for Stormwater Management in Urban Area under Semi-Arid Mediterranean Climate Conditions." Journal of Environmental Management 326(PA):116643.

Radhi, Hassan, Fayze Fikry, and Stephen Sharples. 2013. "Impacts of Urbanisation on the Thermal Behaviour of New Built up Environments: A Scoping Study of the Urban Heat Island in Bahrain." Landscape and Urban Planning 113:47–61.

Rajagopal, Prashanthini, Radhakrishnan Shanthi Priya, and Ramalingam Senthil. 2023. "A Review of Recent Developments in the Impact of Environmental Measures on Urban Heat Island." Sustainable Cities and Society 88(May 2022):104279.

Rasul, M. G., and L. K. R. Arutla. 2020. "Environmental Impact Assessment of Green Roofs Using Life Cycle Assessment." Energy Reports 6:503–8.

Refahi, Amir Hossein, and Hossein Talkhabi. 2015. "Investigating the Effective Factors on the Reduction of Energy Consumption in Residential Buildings with Green Roofs." Renewable Energy 80(12):595–603.

Ren, Zhibin, Yao Fu, Yulin Dong, Peng Zhang, and Xingyuan He. 2022. "Rapid Urbanization and Climate Change Significantly Contribute to Worsening Urban Human Thermal Comfort: A National 183-City, 26-Year Study in China." Urban Climate 43(March):101154.

Rosenfeld, Arthur H., Hashem Akbari, Sarah Bretz, Beth L. Fishman, Dan M. Kurn, David Sailor, and Haider Taha. 1995. "Mitigation of Urban Heat

Islands: Materials, Utility Programs, Updates.” Energy and Buildings 22(3):255–65.

Roth, M., T. R. Oke, and W. J. Emery. 1989. “Satellite-Derived Urban Heat Islands from Three Coastal Cities and the Utilization of Such Data in Urban Climatology.” International Journal of Remote Sensing 10(11):1699–1720.

Rozos, E., C. Makropoulos, and Č. Maksimović. 2013. “Rethinking Urban Areas: An Example of an Integrated Blue-Green Approach.” Water Science and Technology: Water Supply 13(6):1534–42.

Ryu, Young Hee, Elie Bou-Zeid, Zhi Hua Wang, and James A. Smith. 2016. “Realistic Representation of Trees in an Urban Canopy Model.” Boundary-Layer Meteorology 159(2):193–220.

Sabrin, Samain, Maryam Karimi, Rouzbeh Nazari, Joshua Pratt, and Joshua Bryk. 2021. “Effects of Different Urban-Vegetation Morphology on the Canopy-Level Thermal Comfort and the Cooling Benefits of Shade Trees: Case-Study in Philadelphia.” Sustainable Cities and Society 66(September 2020):102684.

Sahani, Jeetendra, Prashant Kumar, Sisay Debele, and Rohinton Emmanuel. 2022. “Heat Risk of Mortality in Two Different Regions of the United Kingdom.” Sustainable Cities and Society 80(January):103758.

Sailor, David J., Timothy B. Elley, and Max Gibson. 2012. “Exploring the Building Energy Impacts of Green Roof Design Decisions-a Modeling Study of Buildings in Four Distinct Climates.” Journal of Building Physics 35(4):372–91.

Saiz, Susana, Christopher Kennedy, Brad Bass, and Kim Pressnail. 2006. “Comparative Life Cycle Assessment of Standard and Green Roofs.” Environmental Science and Technology 40(13):4312–16.

Salata, Ferdinando, Iacopo Golasi, Davide Petitti, Emanuele de Lieto Vollaro, Massimo Coppi, and Andrea de Lieto Vollaro. 2017. “Relating Microclimate, Human Thermal Comfort and Health during Heat Waves: An Analysis of Heat Island Mitigation Strategies through a Case Study in an Urban Outdoor Environment.” Sustainable Cities and Society 30:79–96.

Savi, Tadeja, Anna Dal Borgo, Veronica L. Love, Sergio Andri, Mauro Tretiach, and Andrea Nardini. 2016. “Drought versus Heat: What’s the Major Constraint on Mediterranean Green Roof Plants?” Science of the Total Environment 566–567:753–60.

Sawilowsky, Shlomo S., and R. Clifford Blair. 1992. “A More Realistic Look at the Robustness and Type II Error Properties of the t Test to Departures from Population Normality.” Psychological Bulletin 111(2):352–60.

Sellers, P. J., D. A. Randall, G. J. Collatz, J. A. Berry, C. B. Field, D. A. Dazlich, C. Zhang, G. D. Collelo, and L. Bounoua. 1996. “A Revised Land Surface Parameterization (SiB2) for Atmospheric GCMs. Part I: Model Formulation.” Journal of Climate 9(4):676–705.

Shafique, Muhammad, and Reeho Kim. 2017. “Application of Green Blue Roof to Mitigate Heat Island Phenomena and Resilient to Climate Change in Urban Areas: A Case Study from Seoul, Korea.” Journal of Water and Land Development 33(1):165–70.

Shafique, Muhammad, Reeho Kim, and Daehee Lee. 2016. “The Potential of Green-Blue Roof to Manage Storm Water in Urban Areas.” Nature Environment and Pollution Technology 15(2):715–18.

Sharkey, Thomas D., Carl J. Bernacchi, Graham D. Farquhar, and Eric L. Singsaas. 2007. “Fitting Photosynthetic Carbon Dioxide Response Curves for C3 Leaves.” Plant, Cell and Environment 30(9):1035–40.

Sharma, Richa, and P. K. Joshi. 2016. “Mapping Environmental Impacts of Rapid Urbanization in the National Capital Region of India Using Remote Sensing Inputs.” Urban Climate 15:70–82.

Shuttleworth, W. James, and Robert J. Gurney. 1990. “The Theoretical Relationship between Foliage Temperature and Canopy Resistance in Sparse Crops.” Quarterly Journal of the Royal Meteorological Society 116(492):497–519.

Silva, Cristina M., M. Glória Gomes, and Marcelo Silva. 2016. “Green Roofs Energy Performance in Mediterranean Climate.” Energy and Buildings

116:318–25.

Sinoquet, H., X. Le Roux, B. Adam, T. Ameglio, and F. A. Daudet. 2001. “RATP: A Model for Simulating the Spatial Distribution of Radiation Absorption, Transpiration and Photosynthesis within Canopies: Application to an Isolated Tree Crown.” Plant, Cell and Environment 24(4):395–406.

Taha, Haider. 1997. “Urban Climates and Heat Islands: Albedo, Evapotranspiration, and Anthropogenic Heat.” Energy and Buildings 25(2):99–103.

Taleghani, Mohammad, Laura Kleerekoper, Martin Tenpierik, and Andy Van Den Dobbelsteen. 2015. “Outdoor Thermal Comfort within Five Different Urban Forms in the Netherlands.” Building and Environment 83:65–78.

Tan, Chun Liang, Nyuk Hien Wong, and Steve Kardinal Jusuf. 2013. “Outdoor Mean Radiant Temperature Estimation in the Tropical Urban Environment.” Building and Environment 64:118–29.

Thorsson, Sofia, Fredrik Lindberg, Ingegärd Eliasson, and Björn Holmer. 2007. “Different Methods for Estimating the Mean Radiant Temperature in an Outdoor Urban Setting.” International Journal of Climatology 27(14):1983–93.

Thorsson, Sofia, Joacim Rocklöv, Janina Konarska, Fredrik Lindberg, Björn Holmer, Bénédicte Dousset, and David Rayner. 2014. “Mean Radiant Temperature - A Predictor of Heat Related Mortality.” Urban Climate 10(P2):332–45.

Toparlar, Y., B. Blocken, B. Maiheu, and G. J. F. van Heijst. 2017. “A Review on the CFD Analysis of Urban Microclimate.” Renewable and Sustainable Energy Reviews 80:1613–40.

Tu, Lili, Zhihao Qin, Lechan Yang, Fei Wang, Jun Geng, and Shuhe Zhao. 2017. “Identifying the Lambertian Property of Ground Surfaces in the Thermal Infrared Region via Field Experiments.” Remote Sensing 9(5).

van der Kolk, Henk Jan, Petra van den Berg, Thijs van Veen, and Martijn Bezemer. 2023. “Substrate Composition Impacts Long-Term Vegetation Development on Blue-Green Roofs: Insights from an Experimental Roof and Greenhouse Study.” Ecological Engineering 186(November 2022):106847.

Virk, Gurdane, Antonia Jansz, Anna Mavrogianni, Anastasia Mylona, Jenny Stocker, and Michael Davies. 2015. “Microclimatic Effects of Green and Cool Roofs in London and Their Impacts on Energy Use for a Typical Office Building.” Energy and Buildings 88:214–28.

Wang, Chenghao, Zhi-Hua Wang, and Young-Hee Ryu. 2021. “A Single-Layer Urban Canopy Model with Transmissive Radiation Exchange between Trees and Street Canyons.” Building and Environment 191(December 2020):107593.

Wang, Zhi Hua, Elie Bou-Zeid, and James A. Smith. 2011. “A Spatially-Analytical Scheme for Surface Temperatures and Conductive Heat Fluxes in Urban Canopy Models.” Boundary-Layer Meteorology 138(2):171–93.

Welles, Jon M., and Shabtai Cohen. 1996. “Canopy Structure Measurement by Gap Fraction Analysis Using Commercial Instrumentation.” Journal of Experimental Botany 47(9):1335–42.

Wong, Nyuk Hien, Chun Liang Tan, Dionysia Denia Kolokotsa, and Hideki Takebayashi. 2021. “Greenery as a Mitigation and Adaptation Strategy to Urban Heat.” Nature Reviews Earth and Environment 2(3):166–81.

Wong, S. C., I. R. Cowan, and G. D. Farquhar. 1979. “Stomatal Conductance Correlates with Photosynthetic Capacity.” Nature 282(5737):424–26.

Wright, J. L. 1965. Evaluating Turbulent Transfer Aerodynamically Within the Microclimate of a Cornfield. Cornell Univ.

Yang, Jun, Maigeng Zhou, Zhoupeng Ren, Mengmeng Li, Boguang Wang, De Li Liu, Chun Quan Ou, Peng Yin, Jimin Sun, Shilu Tong, Hao Wang, Chunlin Zhang, Jinfeng Wang, Yuming Guo, and Qiyong Liu. 2021. “Projecting Heat-Related Excess Mortality under Climate Change Scenarios in China.” Nature Communications 12(1):1–11.

Yang, Jun, Qian Yu, and Peng Gong. 2008. “Quantifying Air Pollution Removal by Green Roofs in Chicago.” Atmospheric Environment 42(31):7266–73.

Yin, Chaohui, Man Yuan, Youpeng Lu, Yaping Huang, and Yanfang Liu. 2018. "Effects of Urban Form on the Urban Heat Island Effect Based on Spatial Regression Model." Science of the Total Environment 634:696–704.

Zhang, Yi, Peiyuan Wei, Lei Wang, and Yinghong Qin. 2021. "Temperature of Paved Streets in Urban Mockups and Its Implication of Reflective Cool Pavements." Atmosphere 12(5):1–12.

Zhao, Lei, Xuhui Lee, Ronald B. Smith, and Keith Oleson. 2014. "Strong Contributions of Local Background Climate to Urban Heat Islands." Nature 511(7508):216–19.

Zheng, Xiandi, Fanhua Kong, Haiwei Yin, Ariane Middel, Hongqing Liu, Ding Wang, Tao Sun, and Itamar Lensky. 2021. "Outdoor Thermal Performance of Green Roofs across Multiple Time Scales: A Case Study in Subtropical China." Sustainable Cities and Society 70(March):102909.

Zhong, Zhaoqiang, and Zhiguang Chen. 2022. "Urbanization, Green Development and Residents' Happiness: The Moderating Role of Environmental Regulation." Environmental Impact Assessment Review 97(August):106900.

Zhou, Xilin, Miguel Yamamoto, Shuting Yan, Yasuyuki Ishida, Meng Cai, Qunfeng Ji, Mehdi Makvandi, and Chuancheng Li. 2022. "Exploring the Impacts of Heat Release of Vehicles on Urban Heat Mitigation in Sendai, Japan Using WRF Model Integrated with Urban LCZ." Sustainable Cities and Society 82(April):103922.

Abstract in Korean

그린인프라의 냉각 효과 평가를 위한 3차원 도시 표면 모델 개발

윤 석 환

서울대학교 대학원 협동과정 조경학,

스마트시티 글로벌 융합 전공

지도교수: 이 동 근

전세계적으로 진행되고 있는 도시화는 수많은 문제를 야기하고 있다. 한 가지 두드러진 문제는 도시 열섬 현상으로, 기후 변화로 인해 더욱 심화되고 있다. 이는 도시민의 건강과 생활에 직접적으로 혹은 간접적으로 영향을 미치는 중요한 문제로, 해결하기 위해서는 도시 열 환경을 구성하는 메커니즘을 이해해야 한다. 도시 열 환경은 기후, 도시 형태, 크기, 밀도 및 표면 물질 등 다양한 요인에 따라 달라진다. 따라서 도시마다 다른 열 완화 전략이 필요하며, 복잡한 도시 환경과 냉각 전략에 대한 정량적인 평가가 요구된다.

최근의 연구는 정량적 평가를 위해 측정 연구를 기반으로, 모델

링과 연계하여 한정된 시간과 공간의 단점을 시뮬레이션을 통해 상호 보완하는 방향으로 진행되고 있다 그러나 냉각 효과와 열 환경을 정확하게 시뮬레이션하기 위해서는 다양한 도시 공간을 종합적으로 반영할 수 있는 3차원 도시 캐노피 모델이 필요하다.

본 논문에서는 3D-USM을 개발하여 도시의 열 환경을 진단하고 그린인프라의 냉각 효과를 평가함으로써 냉각 전략에 따른 열 환경 변화를 시뮬레이션 하였다. 첫 번째 장에서는 3D-USM의 개발 알고리즘을 설명하고 주요 매개 변수를 계산하는 효율적인 방법을 제안하였으며, 복잡한 도시 환경을 고려하여 인간의 열 쾌적성에 중요한 요소인 평균 복사 온도(MRT)를 시뮬레이션 하였다.

두 번째 장에서는 다양한 현장 실험과 민감도 테스트를 통해 3D-USM의 실효성과 신뢰성을 확립하였으며, 대표적인 상업지역을 대상으로 도시 열 환경을 진단하고 가로수와 벽면 녹화의 냉각 효과를 정량적인 평가와 동시에 효율적인 식재 배치를 제시하였다. 연구 결과, 가로수는 건축물의 위치와 도로의 방향을 고려한 가로수 식재가 효율적이었으며, 벽면 녹화는 지면 높이에 가까워질수록 냉각 효과가 효율적이었다. 그러나 6 m 이상의 벽면 녹화는 유

의미한 냉각 효과를 제공하지 않아 비용 효율적인 식재 위치와 규모의 필요성을 강조하였다.

세 번째 장에서는 열 저감 효과를 극대화하기 위해 녹색 지붕에 초점을 맞추었다. 저류 옥상 녹화는 옥상 녹화에 저류층을 추가하여 빗물을 저장하고 증발산량을 증가시켜 환경적 편익을 극대화하는 기술입니다. 본 연구에서는 여름철 저류 옥상 녹화의 열 성능을 평가하고 미기후 개선 및 건축물의 냉방 에너지 절감 가능성을 검토하는 데 초점을 맞추었다. 실험군에 따라 토양, 저류층, 식재층의 점진적인 적용을 통해 실험군의 상부 표면 온도와 하부 표면 온도를 측정하고 저류 옥상 녹화의 시너지 효과를 분석하여 개별 및 상호 작용 효과를 평가하였다. 그 결과, 저류 옥상 녹화는 상부 표면 온도에서 최대 7.5℃, 하부 표면 온도에서 최대 17.4℃의 냉각 효과를 나타내어 실내외 열 쾌적성 향상에 가장 큰 잠재력이 보여졌다. 저류 옥상 녹화의 시너지 효과는 상부 −0.80℃, 하부 +1.59℃로 나타났으며, 본 연구에서는 저류 옥상 녹화가 고온 환경에 대응하고 에너지 절감 효과를 동시에 달성하는 혁신적이고 지속 가능한 기술임을 보여주었다.

본 연구는 도시화 및 기후변화로 인해 도시에 당면한 열섬 문제

를 해결하기 위해 3D−USM을 개발하고 효과적인 도시 냉각 전략에 대한 통찰을 제공한다. 도시를 효율적으로 냉각하기 위해서는 도시 환경 조건에 대한 세부 고려가 필요하다. 제안된 3D−USM은 간단한 입력 데이터를 이용하여 복잡한 도시 환경에서 열 현황을 진단하고, 열 쾌적성을 정확하고 효율적으로 시뮬레이션 할 수 있으며, 지속 가능한 도시를 위한 효율적인 냉각 전략을 제공한다.

주요어: 미기후 모델링, 도시 캐노피 모델, 그린 인프라, 평균복사온도, 도시 계획, 실외 환경

학번: 2020-38920

Appendix

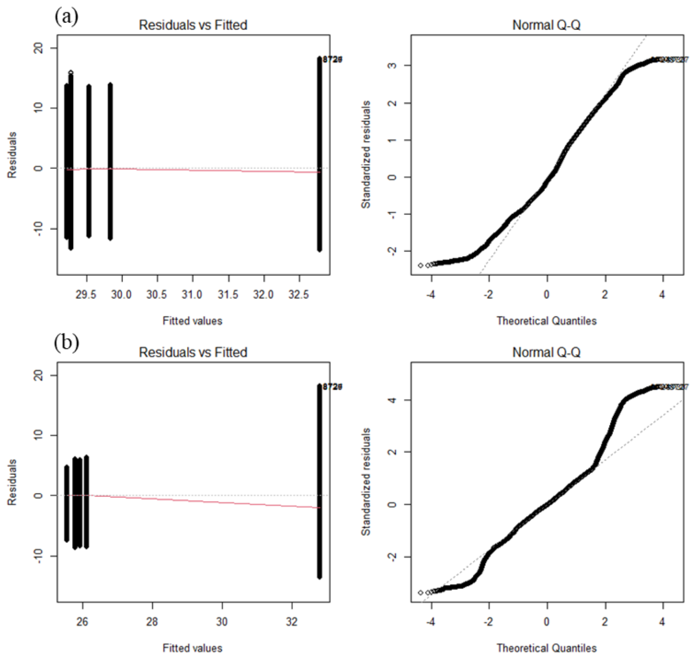

Figure A.1 QQ plot of experimental roofs (a) Upper surface temperature (b) lower surface temperature

(a)

	BG ~ S		G ~ B		BG ~ B		BG ~ G	
Time	P value	T value	P value	T value	P value	T value	P value	T value
00	***	-1.091	ns	0.307	ns	-0.051	ns	-0.358
01	***	-1.004	ns	0.283	ns	-0.048	ns	-0.331
02	***	-0.929	*	0.393	ns	0.042	ns	-0.351
03	***	-0.946	*	0.492	ns	0.112	ns	-0.380
04	***	-0.983	*	0.466	ns	0.083	ns	-0.383
05	***	-0.995	ns	0.409	ns	0.045	ns	-0.364
06	***	-0.923	*	0.479	ns	0.079	ns	-0.400
07	***	-1.016	***	0.930	ns	0.154	***	-0.776
08	ns	-0.271	***	1.109	***	0.790	ns	-0.319
09	***	1.248	***	1.241	***	**1.389**	ns	0.148
10	***	1.650	***	**1.309**	***	1.300	ns	-0.008
11	***	2.089	***	1.273	***	1.272	ns	0.000
12	***	**2.266**	***	1.148	***	1.191	ns	0.043
13	***	2.261	***	1.039	***	1.039	ns	0.000
14	***	1.722	***	0.921	***	0.867	ns	-0.054
15	***	1.020	***	0.741	***	0.628	ns	-0.113
16	ns	0.195	***	0.700	**	0.427	ns	-0.273
17	***	-1.154	***	0.701	ns	0.155	***	-0.546
18	***	-1.483	**	0.474	ns	-0.081	***	-0.554
19	***	-1.520	ns	0.130	ns	-0.350	***	-0.480
20	***	-1.562	ns	0.035	**	-0.446	***	-0.481
21	***	-1.568	ns	0.102	*	-0.384	**	-0.486
22	****	-1.535	ns	0.089	ns	-0.379	**	-0.469
23	***	-1.496	ns	0.142	ns	-0.311	*	-0.453

***p < .001, **p < .01, *p < .05, ns: not significance

(b)

	BG ~ S		G ~ B		BG ~ B		BG ~ G	
Time	P value	T value	P value	T value	P value	T value	P value	T value
00	ns	-0.215	ns	-0.050	***	-0.547	***	-0.497
01	*	-0.304	ns	-0.095	***	-0.591	***	-0.497
02	*	-0.316	ns	-0.143	***	-0.600	***	-0.456
03	**	-0.393	ns	-0.143	***	-0.613	***	-0.470
04	***	-0.452	ns	-0.134	***	-0.636	***	-0.502
05	***	-0.483	ns	-0.125	***	-0.623	***	-0.497
06	***	-0.538	ns	-0.190	***	-0.726	***	-0.536
07	ns	-0.388	ns	-0.147	*	-0.451	ns	-0.304
08	ns	-0.147	ns	-0.118	ns	-0.030	ns	0.087
09	ns	0.108	ns	-0.266	ns	0.227	**	0.492
10	*	0.391	***	-0.444	***	0.487	***	0.931
11	***	0.612	***	-0.714	***	0.664	***	1.378
12	***	0.943	***	**-0.858**	***	0.837	***	1.696
13	***	1.331	***	-0.810	***	0.987	***	**1.797**
14	***	1.746	***	-0.601	***	1.161	***	1.762
15	***	1.947	***	-0.354	***	1.228	***	1.582
16	***	**2.044**	ns	-0.071	***	**1.241**	***	1.311
17	***	2.067	ns	0.153	***	1.174	***	1.021
18	***	1.746	*	0.266	***	0.913	***	0.648
19	***	1.034	**	0.319	***	0.505	ns	0.186
20	***	0.503	***	0.370	ns	0.218	ns	-0.152
21	ns	0.265	***	0.361	ns	0.014	**	-0.347
22	ns	0.129	*	0.289	ns	-0.189	***	-0.477
23	ns	0.021	ns	0.201	*	-0.356	***	-0.557

Figure A.2 Mean difference and significance level (a) upper (b) lower surface temperature between the experimental roof depending over time. (BG: Blue-Green roof, G: Green roof, B: Blue roof, S: Soil roof)

Time	Upper	Lower
00	0.682308	-0.82812
01	0.625208	-0.78352
02	0.620972	-0.74
03	0.677389	-0.69056
04	0.683778	-0.6863
05	0.675787	-0.63704
06	0.602485	-0.72465
07	0.393931	-0.36633
08	0.742308	0.204333
09	0.289817	0.610833
10	-0.35747	1.0275
11	-0.81695	1.430333
12	-1.03158	1.590167
13	-1.2212	1.453282
14	-0.90973	1.176245
15	-0.50476	0.863056
16	-0.04129	0.5075
17	0.763031	0.127639
18	0.847497	-0.18514
19	0.690229	-0.34319
20	0.634962	-0.43694
21	0.697688	-0.59722
22	0.686852	-0.79436
23	0.731811	-0.93409

Figure A.3 Synergy of Greening and blue retention layer, where is calculated by subtracting sum of G-S and B-S with BG-S

(a)

	Soil		Blue		Green		Blue-Green	
Temp	P value	T value	P value	T value	P value	T value	P value	T value
17℃	***	4.07	***	2.01	***	2.31	***	1.69
19℃	***	1.96	***	0.51	***	1.01	***	0.43
21℃	***	3.22	***	2.00	***	2.24	***	1.78
23℃	***	2.96	***	2.21	***	2.62	***	2.23
25℃	***	2.76	***	2.57	***	3.27	***	2.98
27℃	***	3.79	***	3.91	***	4.88	***	4.66
29℃	***	5.42	***	5.35	***	6.28	***	6.17
31℃	***	6.30	***	6.19	***	7.13	***	7.10
33℃	***	6.86	***	7.07	***	7.69	***	7.62

	Soil		Blue		Green		Blue-Green	
RH	P value	T value	P value	T value	P value	T value	P value	T value
30%	***	2.38	***	5.92	***	7.11	***	7.24
40%	***	3.38	***	5.56	***	6.77	***	6.71
50%	***	4.73	***	4.60	***	5.29	***	5.03
60%	***	5.29	***	4.88	***	5.62	***	5.33
70%	***	3.84	***	2.96	***	3.55	***	3.21
80%	***	2.95	***	1.92	***	2.39	***	1.95
90%	***	1.81	***	0.93	***	1.35	***	1.03

(b)

	Soil		Blue		Green		Blue-Green	
Temp	P value	T value	P value	T value	P value	T value	P value	T value
17℃	*	-0.25	ns	0.01	***	0.51	***	0.26
19℃	***	0.76	***	0.90	***	0.93	***	0.77
21℃	***	2.57	***	2.91	***	2.98	***	2.85
23℃	***	4.21	***	4.35	***	4.43	***	4.31
25℃	***	6.63	***	6.92	***	6.79	***	7.16
27℃	***	9.95	***	10.64	***	10.14	***	11.24
29℃	***	12.58	***	13.22	***	12.63	***	13.76
31℃	***	15.29	***	15.72	***	15.03	***	16.39
33℃	***	18.32	***	18.88	***	18.06	***	19.57

	Soil		Blue		Green		Blue-Green	
RH	P value	T value	P value	T value	P value	T value	P value	T value
30%	***	14.08	***	14.68	***	14.33	***	17.51
40%	***	12.87	***	12.39	***	12.62	***	15.18
50%	***	10.51	***	10.73	***	10.56	***	12.00
60%	***	10.14	***	10.85	***	10.40	***	11.42
70%	***	6.15	***	6.67	***	6.48	***	6.82
80%	***	3.72	***	4.05	***	4.01	***	3.67
90%	***	3.13	***	3.33	***	3.23	***	2.72

***p < .001, **p < .01, *p < .05, ns: not significance

Figure A.4 Mean difference and significance level (a) upper (b) lower surface temperature between the Gray roof and the other experimental roof depending on air temperature and relative humidity